Distinct sources for high-K and adakitic magmatism in SE Iran

Monireh Kheirkhah[a], Iain Neill[b]*, Mark B. Allen[c], Mohammad H. Emami[a] and Ali Shahraki Ghadimi[d]

[a]*Research Institute for Earth Sciences, Geological Survey of Iran, Azadi Square, Meraj Avenue, Tehran, Iran*

[b]*Geographical and Earth Sciences, University of Glasgow, Gregory Building, Lilybank Gardens, Glasgow, G12 8QQ, Scotland*

[c]*Department of Earth Sciences, Durham University, South Road, Durham, DH1 3LE, England*

[d]*Geological Survey of Iran, Kerman, P.O. Box 76175-189, Kerman Province, Iran*

*Corresponding author. E-mail: iain.neill@glasgow.ac.uk. Tel: +44 1913 035477.

Abstract

Research into Arabia-Eurasia collision zone magmatism in Kerman Province, SE Iran, has largely focused on Late Cenozoic adakitic stocks or domes, with debate around lower crustal or subducted slab origins. Contemporary hawaiite-trachyandesite lava flows have been overlooked. New analyses for domes and lavas from near Dehaj show major and trace element distributions relating to two distinct compositional series. One contains medium-K domes with SiO_2 > 60 wt.%, high Sr/Y and La/Yb and generally low MgO, Ni and Cr, showing high-silica adakite affinity. The other series has high-K affinity and includes both lavas and dome samples. The two suites partially mixed in the shallow crust, confirmed by fieldwork and petrography. Isotopically the two suites are indistinguishable, implying a geologically 'young' age for the source of the adakites. Given its geochemical signatures and non-relationship with the largely mafic, mantle-derived high-K series, we

consider the adakite series to be derived from melting of eclogitized mafic lower crust. The high-K series relates to dehydration melting of mantle peridotite deeper within the ~220 km thick lithosphere. We also explore adakitic magmas across Iran and their relationship to porphyry copper deposits. At Dehaj and several other Iranian centres, adakites are chemically controlled by garnet as a source or fractionating phase, and are barren, whereas the presence of amphibole as a key phase seems to correlate with Cu mineralisation. This study also shows the need for evidence from multiple datasets to constrain adakite genesis and warns of avoiding sampling bias towards felsic lithologies.

Keywords

Iran, adakite, petrogenesis, collision, magma mixing; mineralisation

1. Introduction

Late Cenozoic magmatism is commonplace across much of Iran, Turkey and the Caucasus (Fig. 1) and results from a variety of geodynamic and petrological processes including Neo-Tethyan slab break-off (Keskin, 2003; Zor et al., 2008), localised lithospheric detachment and sub-lithospheric convection (Kaislaniemi et al., 2014), crustal extension related to strike-slip faults (Sadaat et al., 2010; Shabanian et al., 2012) plus intra-lithospheric breakdown of hydrated peridotite (Allen et al., 2013; Sugden et al., 2019). The diversity of mafic to felsic magmatic products formed in the past few million years is high, ranging from alkaline to sub-alkaline, of within-plate to arc-like chemistry, and moderately to highly enriched incompatible trace element concentrations (Pearce et al. 1990; Saadat and Stern, 2012; Pang et al., 2012, 2013; Kheirkhah et al., 2013, 2015; Allen et al., 2013; Sugden et al. 2019). Many publications on Late Cenozoic samples identify trace element characteristics consistent

with small volume melting of lithospheric mantle previously modified during subduction of the Neo-Tethyan oceanic slab(s) (Pearce et al., 1990; Keskin et al., 1998; Özdemir et al., 2006, 2014; Neill et al., 2015). The extent to which magmas interact with the diverse crustal lithologies also varies considerably but can be reasonably detected in Iran using isotopic data: large parts of the predicted lower crust are ultimately Gondwanan in origin and are sufficiently old to present high $^{87}Sr/^{86}Sr$ and low $^{143}Nd/^{144}Nd$ ratios compared to mantle-derived basalts (Davidson et al., 2004; Ghalamghash et al., 2016; Pang et al., 2012). Such magmatic diversity may also be driven by the region's strongly heterogeneous lithospheric thicknesses, ranging from lithosphere over 200 km thick in the heart of the Zagros core, to less than 50 km in parts of Eastern Anatolia, where mantle lithosphere is very thin or absent (Priestley et al., 2012). Therefore, Iran is a good test site for the identification of sources and processes involved in collision magmatism. It is also important to understand magma genesis in a region where magmatic activity controls mineral resources (Zarasvandi et al., 2015), natural hazards (Karakhanian et al., 2002; Mortazavi et al., 2009), and geothermal energy sources (Seyedrahimi-Niaraq et al., 2017).

One group of rocks which has received special attention in Iran is the adakite series. These volcanic or intrusive lithologies have attracted much controversy over their definition, petrogenesis, and implications for the occurrence of porphyry Cu mineralisation (e.g. Jahangiri, 2007; Omrani et al., 2008; Aftabi and Atapour, 2009; Khodami et al., 2009; Shafiei et al., 2009; Richards et al., 2012; Asadi et al., 2014; Azizi et al., 2014; Zarasvandi et al., 2015; Pang et al., 2016; Shaker Ardakani, 2016; Lechmann et al., 2018). Omrani et al. (2008), Pang et al. (2016) and Shaker Ardakani (2016) described Late Cenozoic adakite-like felsic rocks in Kerman Province and elsewhere in Iran (Fig. 1) and argued that these magmas formed due to melting of the Neo-Tethyan slab beneath the collision zone (Omrani et al., 2008), or by melting of existing arc rocks in the lower crust (Pang et al., 2016). We present new

geochemical data from around Dehaj in Kerman Province which are used to a) debate the origins of the adakitic signature, b) link the origin of the adakites to what is known about contemporaneous non-adakitic magmatism and the crustal and lithospheric thickness in Kerman Province and c) identify any geochemical patterns across the regional distribution of adakitic magmatism and its correlation with porphyry copper mineralisation.

2. Geological background

2.1. Regional geological setting

Kerman Province is part of the Turkish-Iranian Plateau, the latter an area of ~1.5 M km^2 and ~1.5-2 km elevation within the Arabia-Eurasia collision zone (Agard et al., 2011). The plateau was created by the collision and postdates the extensive marine limestones of the Late Oligocene - Early Miocene Qom Formation and lateral equivalents (Reuter et al., 2009). Plateau elevations are partly an isostatic response to crustal thickening, but other mechanisms may include the influence of warm and low-density upper mantle (Maggi and Priestley, 2005), and the rise of the under-thrust Arabian plate after slab break-off (Bottrill et al., 2012). Most of the plateau lies within the Eurasian plate (Agard et al., 2005). There is presently little internal strain within the plateau, contrasting with continued thrusting and crustal thickening in the lower elevation parts of the Zagros, and in the Alborz mountains on the north side of the plateau (Jackson et al., 1992; Vernant et al., 2004). Initial collision may have begun at ~25-35 Ma (Allen and Armstrong, 2008; McQuarrie and van Hinsbergen, 2013) and continues to the present day. The GPS-derived velocity field shows roughly 20 mm/yr of north-south convergence (Vernant et al., 2004). The thickness of the lithosphere under Iran now exceeds 200 km adjacent to the Zagros suture (Priestley et al., 2012), thinning towards the margins of the collision zone.

Crustal thickness is likewise variable, from ~40-60 km (Seber et al., 2001; Taghizadeh-Farimand et al., 2015). From these three studies the crustal thickness is around 50 km in the Dehaj study area, and the lithosphere is likely to be 220 ± 50 km thick.

Today's Iranian crust is built around the Central Iranian Microcontinent (CIM), widely considered to be part of a rifted terrane of Gondwanan origin called Cimmeria (Şengör et al., 1988). The western parts of Iran, on the western margin of the CIM, contain the Urumieh-Dokhtar Magmatic Arc (UDMA) and the Sanandaj-Sirjan Zone (SaSZ), which are crustal belts affected by Neo-Tethyan subduction processes from the Jurassic to the present (Hassanzadeh and Wernicke, 2016). The SaSZ is a Gondwana-derived terrane accreted to the rest of Iran during Palaeozoic Palaeo-Tethyan subduction (Stampfli and Borel, 2002), and it preserves a modest record of Neo-Tethyan subduction-related magmatism, particularly during the Jurassic and Eocene (Deevsalar et al., 2017). In contrast, the UDMA had an upsurge in magmatic activity during the Paleocene - Eocene as a result of Neo-Tethyan slab roll-back, tearing and back-arc extension (Verdel et al., 2011; Deevsalar et al. 2018). A comparatively quiescent phase occurred during the Oligocene and much of the Miocene, contemporary with the developing Arabia-Eurasia collision (Chiu et al., 2013; Kaislaniemi et al., 2014). In the last few million years, magmatism has been abundant in eastern Anatolia, the Caucasus and NW Iran, probably related to the thin lithosphere reported from this area (Keskin, 2003; Zor et al., 2003). Otherwise, scattered magmatic centres are developed across the collision zone, up to 700 km from the original Bitlis-Zagros suture (Shabanian et al., 2012; Kheirkhah et al., 2015; Pang et al., 2012). Volcanism in the Dehaj region, in the southwest of the UDMA (Figure 1), is part of this late Cenozoic magmatism. The Dehaj rocks are underlain by Neogene and Eocene volcanic and intrusive material (Soheili, 1981).

The cause of this Late Cenozoic collision zone magmatism is debated. Major geodynamic re-organisations involving breakoff of the subducted Neo-Tethyan oceanic slab and/or detachment of the lower lithosphere have been proposed (Pearce et al., 1990; Keskin, 2003; Omrani et al., 2008). In support of this argument, detached slabs have been interpreted from tomographic images (Hafkensheid et al., 2006), corroborating predicted and observed uplift patterns (Francois et al., 2014; Magni et al., 2017). There is some debate over the specific timing of slab breakoff during the Late Cenozoic (Chiu et al., 2013). However, magmatism has seemingly persisted for several to tens of millions of years following break-off, prompting Kaislaniemi et al. (2014) to propose small scale sub-lithospheric convection as an additional trigger for magmatism. They argued that hydrated lithospheric mantle would be prone to dripping into the underlying asthenosphere, causing convection and melting of upwelling asthenosphere and potentially the down-going lithosphere. Allen et al. (2013) and Sugden et al. (2019) also proposed that melting within the mantle lithosphere could be triggered by the breakdown of hydrous phases such as amphibole.

2.2 The origin of adakitic magmas

As noted in Chapter 1, rocks of adakitic affinity are an important component of Late Cenozoic collision magmatism. These have been identified widely across Iran, with petrogenetic interpretations split between slab melting (e.g. Omrani et al. 2008), melting of crustal lithologies (e.g. Lechmann et al., 2018) and fractional crystallisation of more mafic precursor magmas (e.g. Richards et al. 2012). Adakites are defined as intermediate to felsic volcanic or intrusive samples typically containing high SiO_2, Al_2O_3, Na_2O, Sr, Sr/Y and La/Yb, low K_2O, MgO, K_2O/Na_2O, Y and Yb (e.g., Defant and Drummond, 1990; Defant et al., 1991; Martin, 1999; Castillo, 2012). There are high- (>60 wt.% SiO_2) and low-silica (<60 wt.% SiO_2) varieties, with higher MgO, Ni and Cr in low-silica adakites,

interpreted as a proxy for interaction between adakitic magmas and mantle wedge peridotite (Martin & Moyen, 2003; Martin et al., 2005). At least some adakites or 'adakite-like' rocks are associated with large porphyry Cu-Mo deposits (e.g., Li et al., 2011; Richards et al., 2012) and adakites may be chemically similar to Archaean felsic crust (e.g., Martin, 1999; Martin et al., 2005; Hastie et al., 2015). Various authors initially proposed that modern adakites are generated by the melting of young, hot oceanic crust in subduction zones or at slab edges (e.g., Defant and Drummond, 1990; Peacock et al., 1994).

Following the initial popularity of the slab melting model, other petrogenetic processes have been proposed to produce adakitic geochemical signatures (Moyen, 2009; Castillo, 2012; Richards et al., 2012). For example, the suppression of plagioclase fractionation in hydrous magmas causes Sr to behave incompatibly, increasing Sr/Y ratios to higher values than in typical arc rocks as magmas evolve (Richards, 2006; Richards 2011). Garnet fractionation produces depleted heavy rare earth element (REE) values and hence high light/heavy (LREE/HREE) ratios, because of their partitioning behaviour in the mineral ($D_{LRR<HREE}$) (Kay et al., 1987; Macpherson et al., 2006; Rodriguez et al., 2007; Chiaradia et al., 2009). Amphibole fractionation also produces low Y and high Sr/Y values but should be distinguishable from garnet involvement as the MREE partitioning behaviour varies between the two (amphibole $D_{MREE>HREE}$, garnet $D_{MREE<HREE}$) (Richards and Kerrich, 2007; Rooney et al., 2011; Davidson et al., 2013; Chen et al., 2016). Melting of under-plated or in-situ mafic lower crust containing garnet and/or amphibole can produce similar overall trace element patterns to pristine slab melts unaffected by mantle interaction (e.g. Atherton and Petford, 1993; Pe-Piper and Piper, 2001; Chung et al., 2003; Guan et al., 2012; Xu et al., 2015).

Adakite-like rocks cannot be treated in isolation when determining their petrogenesis. For example, the presence of contemporary mafic magmatism indicates concurrent mantle melting processes which may rule out the possibility of pristine slab melts reaching crustal levels. At Dehaj, we have identified that past work has not involved detailed analysis of a suite of mafic lavas that appear to be contemporary to the known rocks of adakitic affinity. Though based on a relatively small new sample set, we re-open the debate over the origin of magmatism at Dehaj, and the origin of adakites more generally in Iran.

3. Sample descriptions and analytical methods

We collected 13 samples from the vicinity of Dehaj in Kerman Province, SE Iran (Figure 2) for whole rock elemental and isotopic geochemistry. Shaker Ardakani (2016) described trachyandesitic to trachydacitic subvolcanic 'domes' generally of felsic composition, but also containing more mafic enclaves or distinct more mafic facies with evidence for mingling and/or mixing of two distinct magma types, and which they included in their geochemical analyses. However, hawaiite to trachyandesite lavas also occur in the area, which this paper demonstrates are geochemically similar to the more mafic intrusive rocks. Eight of our samples are from these lavas which are found to the west of the Kuh-e-Aj-Bala dome (~51-61 wt.% SiO_2). These lavas (Figure 3) were initially mapped as Pliocene-Quaternary (Soheili, 1981), but later assumed to be of Upper Miocene – Pliocene age based on local field relationships (Omrani et al., 2008). Five samples are from the subvolcanic domes or 'stock' of Kuh-e-Aj-Bala (Figure 3). Pang et al. (2016) used secondary ionisation mass spectrometry to determine ages of between 1.15 ± 0.03 and 2.15 ± 0.08 Ma (2σ) for three samples from this location. Though we would prefer to have Ar/Ar geochronology for the lavas, the geochemical similarity of previously analysed less evolved samples from the domes and our new lava analyses lends weight to the

192 contemporaneous nature of intrusive and extrusive magmatism (see Results, below; Table 1) (Shaker
193 Ardakani, 2016). In summary, the intrusive and extrusive rocks analysed here formed within the last
194 several million years, and they come from a restricted geographic range (Figure 2) which makes it
195 important to consider their petrogenesis in relationship to each other.
196
197 For full analytical methods for major and trace element determinations, see Neill et al. (2013),
198 which includes full trace element standard analyses run at the same time as this sample set. Sample
199 preparation was conducted at Durham University. X-ray fluorescence analysis for major elements was
200 done at the University of Leicester using a PANalytical Axios Advanced spectrometer, and trace
201 element solution chemistry at Durham University used a Thermo X2 inductively coupled plasma mass
202 spectrometer (ICP-MS). During the Dehaj sample run, Standard W2 (n = 15) gave first relative
203 standard deviations of 5% or better for all transition metals (10% for Sc, 12% for Cr, 6% for Ni), the
204 large ion lithophile elements (LILE), high field strength elements (HFSE) and the REE; excepting 7%
205 for La, 6% for Ce. Results are presented in Table 1, including sample locations. Radiogenic isotope
206 analysis at the Durham Geochemistry Centre took place as reported fully in Kheirkhah et al. (2013).
207 Nd-Sr radiogenic isotopes were analysed on a Thermo Neptune Multi-Collector ICP-MS. During the
208 Dehaj run, Sr blanks averaged 88 pg (n = 6). Standard NBS987 gave a mean $^{87}Sr/^{86}Sr$ of 0.710263 ±
209 12 (2σ, n = 12, minimum uncertainty 16 ppm) [corrected to a preferred value of 0.710240]. Nd blanks
210 averaged 10 pg (n = 6). The Sm-doped and un-doped versions of the J&M standard gave a mean
211 $^{143}Nd/^{144}Nd$ of 0.511099 ± 4 (2σ, n = 26, minimum uncertainty 7 ppm) [corrected to a preferred value
212 of 0.511100]. Results are presented in Table 2.
213
214 **4. Results**
215

4.1. Petrography

The lavas have plagioclase, rare olivine, and clinopyroxene phenocrysts, set in a fine-grained to glassy groundmass (e.g. Figure 4a). Some of the olivine crystals have dark red brown iddingsite rims. The groundmass contains plagioclase, olivine, clinopyroxene, rare K-feldspar and opaque minerals. There are a few xenocrysts of quartz in sample DJ25.5, with reaction rims surrounding pyroxene needles in the groundmass, indicating interaction of more mafic magma with a more silicic component. Rare accessory phases include titanite and apatite. Some samples contain glomerocrysts, for example in DJ2.1 (Figure 4b). The more acidic samples also have porphyritic textures, both in the lavas and intrusive rocks (Figure 4c). The phenocrysts in the intrusive samples are mostly plagioclase (andesine, with common zoning and rarer sieve texturing), with subordinate idiomorphic–hypidiomorphic green to brown hornblende, rare tabular K-feldspar (sanidine) and quartz. Hornblende phenocrysts are mostly green and may be strongly oxidized or have iron oxide rims. Quartz phenocrysts are rounded. The groundmass in the intrusive samples is mainly composed of feldspars (sanidine and plagioclase), quartz and hornblende, with apatite, biotite and iron oxides as accessory minerals.

4.2. Elemental geochemistry

New geochemical results are presented in Table 1, with associated diagrams supplemented by the analyses of intrusive rocks by Pang et al. (2016) and Shaker Ardakani (2016). We begin by segregating samples by intrusive vs extrusive nature (lava vs dome) and author but identify two magmatic series which form a basis for later diagrams and discussion (Figure 5). Pang et al. (2016) focus entirely on evolved dome samples, whereas Shaker Ardakani (2016) included more mafic facies

or enclaves from within the domes. The earlier published dataset of Omrani et al. (2008) is equivalent to Pang et al. (2016) and hence omitted here.

Most of our samples have very low loss on ignition, but values of 1.9-2.8 % were returned for mafic lavas DJ6.1, DJ25.1 and DJ25.5, those which contained the highest Sr (>3000 ppm) of our sample set. At this modest loss on ignition we do not expect disturbance of immobile element concentrations and ratios, but very high Sr perhaps indicates accumulation of plagioclase feldspar and subsequent alteration to clay minerals, or accidental incorporation of Sr-rich amygdales, despite screening during sample preparation. We highlight these samples on relevant diagrams and are mindful not to involve them in discussion where appropriate.

Our extended dataset, including the lavas, demonstrates a broad compositional spectrum in the sample set from hawaiite lava (~51 wt.% SiO_2) to rhyolitic intrusive rocks (~72 wt.% SiO_2), crossing the alkaline to sub-alkaline divide (Figure 5a). The most mafic lava has MgO of ~6%, with 140 ppm Ni and 320 ppm Cr (Table 1), not clearly representing a primary magma. When shown on a K_2O vs. SiO_2 plot the sample set splits into two more obvious magmatic series (Figure 5b). First, the hawaiite to trachyandesite lavas and more mafic of the intrusive rocks form a high-K trend, whereas most of the remaining intrusive samples fall in a medium-K trend. A few samples, including both intrusive rocks and lavas, are intermediate between the two trends and are here termed ‘transitional’. All samples have a sodic character, however, with $NaO > K_2O$ (Table 1). An immobile element Th-Co diagram (Hastie et al., 2007) rules out sub-solidus mobilisation of K_2O as responsible for the high- and medium-K trends: one trend consists of shoshonitic basalts through to dacites (the high-K trend), and one more clustered set of points consists almost exclusively of evolved calc-alkaline compositions (the medium-K trend) (Fig. 5c). The same transitional samples plot between the two trends on the Th-Co plot. On

some Harker plots (Fig. 5d-h), such as for MgO, Sr and Y (Figures 5d, g, h), the series overlap, falling on the same overall trends. For example, there are general trends between Sr and Y and SiO_2, suggestive of fractional crystallisation involving plagioclase, and with Y behaving compatibly throughout the evolution of the two magma series. The plots of Ni and Cr vs SiO_2 and of Rb vs SiO_2 do show the distinction between the series, with the medium-K series always having much lower Ni and Cr concentrations and Rb behaving incompatibly in the high-K series but with D≈1 in the medium-K samples (Figures 5e, f).

The intrusive, medium-K samples have high Sr/Y such that they fall within the adakitic field on a Sr/Y v Y plot, corroborating previous findings of adakitic compositions (Figure 6a). As such, from now on we refer to these samples as belonging to the 'adakite' series. The high-K samples are demonstrably not adakitic, which is a new finding for this area, including the three high-Sr lavas (Figure 6a). There is a rough correlation for both series between Sr/Y ratios and SiO_2 (Figure 6b), indicating that fractionation may play a role in generating or maintaining the high Sr/Y signatures, as implied by the Sr v SiO_2 and Y v SiO_2 plots (Figure 5). A similar pattern is shown on a plot of La/Yb_{CN} v Yb_{CN} (CN = chondrite-normalised, values from McDonough & Sun, 1995; Figure 6c), where the high-K series does not plot within the adakitic field. There is a correlation in the adakite series between La/Yb_{CN} and SiO_2, implying a role for fractionation in maintaining the adakitic signature. The transitional samples which fall between the two series accordingly lie on the divide between adakitic and non-adakitic compositions on both plots. Of the adakitic samples, SiO_2 is >60 wt.%, MgO generally <3 wt.%, Ni and Cr <20 ppm and Sr >500 ppm even in the least evolved samples. As such, these rocks classify as high silica adakites (Martin & Moyen, 2003).

On a chondrite-normalised diagram (Fig. 7a), the high-K hawaaite-trachyandesite series has the highest overall abundance of REEs, with moderately steep REE patterns (La/Yb_{CN} = 12-25) and around 100 to 200 times chondrite for the light REE and about 10 times chondrite for the HREE. Slight negative Eu anomalies are present (geometric Eu/Eu* = 0.82-0.93) implying a role for plagioclase fractionation in petrogenesis. The adakite series has lower REE concentrations with steeper patterns compared to the high-K series (La/Yb_{CN} = 21-89) and a greater spread of HREE depletion between 1-9 times chondrite. The Eu/Eu* ratios vary between 0.82 and 1.18, perhaps linked to the generally intrusive nature of the suite and the potential for sampling of both plagioclase-depleted and plagioclase-accumulative zones within the domes. The transitional samples again lie between the two series. Primitive Mantle-normalised trace element plots also demonstrate that samples share some common features (Figure 7b-d). These include a positive anomaly for Sr, even ignoring the samples with the highest abundances, but negative Nb, Ta, P and Ti anomalies. A modest negative anomaly for Zr appears in some samples which may indicate the onset of Zr saturation. The average member of the high-K series is considerably more enriched in large ion lithophile elements (LILE), e.g., Sr, Ba and Th; however, the high-K series contains similar K and lower concentrations of Rb relative to the adakites.

4.3. Radiogenic isotope geochemistry

The five samples analysed for Sr-Nd isotopes in this study include three adakites and two high-K series samples. They fall within a limited compositional range (Table 2) predominantly in the depleted quadrant with respect to Bulk Earth and within the mantle array (Figure 8). Including two adakitic samples of Omrani et al. (2008) and six of Pang et al. (2016), the measured $^{87}Sr/^{86}Sr$ ranges from 0.7040 to 0.7058, and $^{143}Nd/^{144}Nd$ from 0.5128 to 0.5129. Some samples fall to the right of the

mantle array at high $^{87}Sr/^{86}Sr$ but invariant $^{143}Nd/^{144}Nd$, suggestive of sub-solidus alteration as opposed to interaction with isotopically evolved continental crust. Few Eocene rocks of the UDMA have been analysed from the local area – four samples of Omrani et al. (2008) trend towards much lower $^{143}Nd/^{144}Nd$ than the Quaternary Dehaj samples (0.5125-0.5129). More widely in the collision zone, the Dehaj rocks are isotopically quite similar to lavas considered to represent melting of peridotite or pyroxenite within the lithospheric mantle across the Lesser Caucasus (Neill et al., 2015). The Dehaj rocks, including the adakites, are derived from an isotopically quite depleted source which has not interacted with large volumes of in situ old continental lithosphere or old subducted crust.

5. Discussion

5.1. Petrogenesis of the high-K series

The presence of high-K mafic to intermediate lavas, plus enclaves within the domes (Shaker Ardakani, 2016) indicates a mantle source for at least some of the magmatism at Dehaj. In three recent studies (Omrani et al., 2008; Shaker Ardakani, 2016 and Pang et al., 2016), authors argued that either slab or lower crustal melting was the source of adakitic magmatism in the Dehaj area. However, there was no discussion about the origins or geological implications of contemporaneous mantle-derived magmatism. Below, the petrogenetic characteristics of the high-K series are discussed. As the majority of these rocks are trachyandesitic in composition, no detailed petrogenetic modelling was attempted.

Firstly, amphibole has been widely implicated in the source or fractionation history of mafic lavas across the Turkish-Iranian Plateau, as a marker for subduction-modified mantle sources of hydrous magmatism (e.g. Pearce et al., 1990), and we first seek to determine its role in the petrogenesis of the

high-K series. Further, distinguishing if magmas originated within the garnet and/or spinel peridotite facies constrains the depth of melting due to the transition between these phases at ~75 km depth in the mantle. To determine the relative roles of amphibole, garnet and spinel we look to REE systematics. It is generally accepted that Dy is more compatible in amphibole relative to garnet, and vice versa for Yb (Davidson et al., 2013) whereas spinel is compatible in neither. Davidson et al. (2013) proposed that the Dy/Dy* ratio could be a proxy for residual amphibole during melting or its fractionation during magma evolution. In the high-K series there is no relationship between Dy/Yb ratios and SiO_2 (Figure 9a). On a Dy/Dy* vs Dy/Yb plot, the high-K series follows a shallow trend not consistent with amphibole fractionation or residual amphibole but showing control from garnet, probably as a residual phase given the non-relationship between Dy/Yb and SiO_2 (Figure 9a). The sample showing the least amphibole or garnet control, mafic sample B-14 of Shaker Ardakani (2016), has La/Yb of 26 and Dy/Yb of 2.1. On the plot of Sugden et al. (2019), this sample falls in the Syunik Province and Gegham Ridge fields from southern Armenia (where the lithosphere is >100 km thick with ~45 km crustal thickness). This diagram implies that the high-K series may be derived from very small volume melting (~0.1 to 1 %) just within the garnet-spinel transition zone (Figure 9b), i.e. towards the top of the mantle lithosphere beneath Dehaj.

The Zagros suture lies ~150 km to the SW and there is no documented geophysical evidence for a subducted slab within the lithospheric mantle. Any subduction-related geochemical component is therefore most likely to have been inherited from previous subduction episodes. As noted, the hawaiite-trachyandesite high-K series is LREE- and LILE-enriched, with large negative Nb-Ta anomalies on Figure 7b. The La/Nb ratio ranges from 2.2 to 4.6, indicating a source which experienced a significant contribution from a subduction-related fluid and/or melt. On a Th/Yb vs. Ta/Yb plot (Pearce, 1983), the least evolved of the high-K series samples also fall within the subduction-modified, enriched-source

358 shoshonitic field (Figure 10a). There is no relationship between Yb and SiO_2, so highly incompatible
359 behaviour of Th in the evolving magma seems to be a dominant factor in this variation rather than a
360 specific source control. An additional consideration in understanding the mantle source comes from
361 Rb, Sr and Ba systematics. Different trends on a Rb/Sr vs Ba/Rb plot (Furman & Graham, 1999) have
362 been interpreted in terms of residual phlogopite (high Rb/Sr ratios) or amphibole (high Ba/Rb ratios)
363 based on the respective Kd values in these minerals (Figure 10b). The Dehaj mafic high-K samples all
364 lie on the amphibole trend. Even excluding samples with anomalously high Sr concentrations, there is
365 no trend between Ba/Rb ratios and SiO_2. This finding confirms the presence of residual amphibole in
366 what is therefore a hydrated mantle source, but also confirms the finding from REE systematics that
367 amphibole fractionation is not important. Finally, some trace element ratios help determine if sediment-
368 related melt or fluid release was responsible for metasomatizing the mantle source of the high-K series.
369 There is no relationship between the ratios of Th/Nb, La/Nb and Ba/Nb and SiO_2, so these are
370 considered reflective of source and partial melting conditions and have been applied to the diagrams of
371 Zamboni et al. (2016). Supercritical fluids related to subducting slabs tend to have enrichments in La
372 and Ba relative to sediment melts which have higher concentrations of Th. The Dehaj high-K series
373 plots roughly between the two trends, implying a source influenced by a combination of both fluid and
374 partial melt (Figures 10c and 10d).
375
376 5.2. The origin of the adakite series
377
378 Given past disagreement over the origin of the adakite series both at Dehaj and more widely across
379 Iran, we now review petrogenetic evidence from the new and existing adakite geochemistry at Dehaj,
380 considering the presence of contemporary mantle-derived magmatism.
381

382 *5.2.1. Deep slab melting?*

383

384 There is no geochemical evidence for interaction between the least-evolved of the high-K series
385 and deeper, upwelling magmas derived from partial melting of a subducting slab. The two distinctive
386 magma series can be clearly identified on major and trace element diagrams (Figure 5). The high-K
387 series extends to low SiO_2 values and maintains high Ni and Cr concentrations which would be diluted
388 if there were significant interaction with adakitic slab melts. The adakite series, regardless of SiO_2
389 concentrations (62-71 wt.%) has consistently low MgO (<2 wt.%), Ni (<13 ppm) and Cr (<20 ppm)
390 concentrations which are characteristic of high silica adakites which have not interacted with mantle
391 peridotite on their way to the surface (Moyen, 2009).

392

393 The rock samples classed as 'transitional' are interpreted here as the product of mixing between
394 the high-K and adakitic magmas. Is it possible that these transitional samples were slab melts which
395 interacted with mantle-derived melt at mantle depths? This is unlikely for two reasons. Firstly, there is
396 field evidence in Shaker Ardakani (2016) for mingling of the high-K and adakite series magmas at sub-
397 volcanic depths. Secondly, transitional samples are confined to a narrow range of 60-62 wt.% SiO_2 and
398 do not display any evidence of fractional crystallisation in their own right. Should these transitional
399 magmas have been generated at mantle depths, shallower crustal magmatic evolution would occur in
400 that series, generating a greater spread of SiO_2 for transitional compositions. As such, we cannot
401 identify evidence from any of the erupted or emplaced rocks of interaction between slab melts and the
402 mantle or mantle-derived magmas.

403

404 Finally, at a distance of ~150 km from the Zagros Suture, and with tomographic evidence for a
405 detached Zagros slab within the asthenosphere beneath the collision zone (van der Meer et al., 2018), it

406 seems unlikely that any slab material is physically present within the mantle lithosphere beneath
407 Kerman Province. We therefore rule out the hypothesis of Omrani et al. (2008).
408
409 *5.2.2. Fractional crystallisation of a mafic parent?*
410
411 The high-K series is the only mafic to intermediate magmatism for which there is surface evidence of
412 contemporaneous formation with the adakites. We have no reason to suspect the presence of any other
413 potential mafic precursors to the adakites. The high-K and adakite series are clearly geochemically
414 distinct and the former cannot be parental to the latter. Firstly, the high-K series has a greater
415 concentration of most incompatible elements relative to the adakites (Table 1). The high-K series also
416 has higher $^{87}Sr/^{86}Sr$ and lower $^{143}Nd/^{144}Nd$ compared to that of many of the adakites (Figure 8).
417 Therefore, any assimilation-fractional crystallisation model would require that the high-K series be
418 contaminated by isotopically depleted, medium- to low-K crust. Geologically this is not a feasible
419 scenario given the known compositions of the continental crust and of Eocene and younger magmatism
420 in the region. Finally, there are no adakites lower than ~62 wt.% SiO_2, and the low MgO and transition
421 metal concentrations within the adakite series do not belong to the same geochemical trend as the most-
422 evolved of the high-K series (Figure 5). Therefore, a fractional crystallisation origin for the adakites
423 from this mafic, mantle-derived parental magma is not likely.
424
425 *5.2.3. Melting mafic lower crust: in situ or delaminated?*
426
427 Next, we consider if the adakites are derived from melting of a crustal lithology perhaps at the base of
428 the UDMA crust. The adakites are isotopically depleted and there is no positive relationship between
429 $^{87}Sr/^{86}Sr$ and the degree of magma evolution. Therefore, if the adakites are ultimately sourced from the

melting of crustal lithologies, that crust must not be ancient or otherwise isotopically evolved but should have formed in the recent past. Geologically this is feasible: subduction of the southern branch of the Neo-Tethys ocean led to subduction-related magmatic episodes from the Mesozoic to the early Eocene, followed by the Late Eocene emplacement of within-plate magmas during Neo-Tethyan slab roll-back (Verdel et al. 2011; Deevsalar et al. 2018). It is reasonable to assume that young mafic lower crust, perhaps underplated, lies beneath Dehaj.

Clemens et al. (2006) demonstrated that plagioclase is stable within the crust to about 1.5 GPa, or approximately 50 km. At shallower depths, the presence of residual plagioclase during partial melting is likely to result in the production of low-Sr (<400 ppm) magmas (Smithies et al., 2009). In our sample set and the analyses of Shaker Ardakani (2016) and Pang et al. (2016), Sr concentrations in the adakites are consistently > 400 ppm, and those adakites which are least evolved, containing ~60-64 wt.% SiO_2, have 800-1800 ppm Sr. This finding is a pointer towards either the complete dissolution of plagioclase during partial melting at amphibolite facies, or its absence during melting within the deeper eclogite facies at >50 km. It would represent an unusually high degree of melting for plagioclase to be completely consumed from a crustal amphibolite which might contain many tens of % plagioclase. Furthermore, as there is only evidence for small volumes of mafic, mantle-derived magma (the high-K series), heat advection is unlikely to be a strong driver of extensive lower crustal melting. It is also unlikely that the source would be a plagioclase-poor lithology such as a mafic to ultramafic cumulate, especially as the melting temperature of such a rock would be high and therefore other plagioclase-bearing lithologies would also melt out, generating low-Sr non-adakitic magmas. It seems much more likely that plagioclase was absent in the source rock and that the source was therefore transitioning to, or within, the eclogite facies.

Recent determinations indicate the UDMA crust beneath Dehaj to be approximately 50 km thick (see Section 2), on the cusp of formation of eclogite. Allowance must be made for uncertainty in crustal thickness models, so the simplest explanation for generation of adakitic magmas in this setting is that the lowermost crust partially melted during the amphibole-eclogite transition, aided by the fact this was taking place at the thermal boundary with the underlying mantle. Should the crust in reality be somewhat *thinner* than 50 km, others such as Lechmann et al. (2018) have proposed that, during the ongoing Arabia-Eurasia collision, slivers of garnet amphibole were torn from the base of the Iranian crust and tectonically interwoven with the lithospheric mantle. These crustal fragments would therefore be subjected to higher pressures and temperatures than at the Moho, converting to eclogite facies, at which point dewatering and partial melting could take place. Lechmann et al. (2018) proposed this model to explain why adakites in NW Iran, which require an eclogitic source, were generated in a region of thinner orogenic crust (~45 km) without slab melting. Lechmann et al. (2018), like us, considered a fractional crystallisation model difficult to reconcile with local geological evidence. Alternatively, it is possible that crustal thickening during collision can 'eclogitize' mafic lower crust, to the point where it becomes seismically less distinguishable from the surrounding mantle (e.g. Dewey et al. 1993). This model allows for the crust to be *thicker* than geophysical estimates allow, giving us more confidence that the lower crust can be a source of the adakitic series. Therefore, we have confidence that melting of eclogitic rocks took place at >50 km and at shallower depths than the beginning of the onset of the spinel-garnet transition in mantle lithologies.

5.3. Fractional crystallisation vs the strength of the adakitic signature

Regardless of the source model, we have already noted that the evolution of the adakite series from ~60-72 wt.% SiO_2 includes sharp upturns in La/Yb and a steady increase in Sy/Y ratios (Figure

6b, d). Therefore, two iconic signatures of adakitic magmatism show a direct relationship with the degree of magma evolution. On Figure 9a, there are very variable Dy/Yb ratios consistent with the involvement of garnet, and that ratio becomes greater the more evolved the adakites are. This finding strongly implies a garnet control during fractional crystallisation which modifies the adakite signature at Dehaj. Garnet, the only major phase capable of strongly fractionating the heavy REE, must fractionate at depth as no garnet is physically seen in the petrography. Secondly, although Sr behaves compatibly, indicating plagioclase fractionation, the Sr/Y ratio is largely controlled by garnet compatibility in Y. The narrow range of Dy/Dy* ratios in the adakites (Figure 9a) also implies no strong role for amphibole during magma evolution. In short, garnet is a major player in the evolution of the Dehaj adakite signature.

We also consider the geochemistry of other late Cenozoic igneous suites from across Iran and adjacent areas. Several of these have previously been reported as having adakitic compositions (Jahangiri, 2007; Omrani et al., 2008; Khodami et al., 2009; Shafiei et al., 2009; Richards et al., 2012; Shabanian et al., 2012; Azizi et al., 2014; Asadi et al., 2014; Ghorbani et al., 2014; Zarasvandi et al., 2015; Lechmann et al., 2018), mainly from middle and Late Miocene centres. The youngest (Quaternary) centres, and some Late Miocene centres, lack detailed reports of adakitic compositions (e.g. Kheirkhah et al., 2009; Allen et al., 2013), although evolved rocks were not always the focus in some of these works, and Pang et al. (2016) and Lechmann et al. (2018) both noted several <5 Ma volcanic centres in northwest Iran, Armenia and Georgia as having adakitic compositions. Late Cenozoic adakitic rocks seem to be rarer in the western parts of the Arabia-Eurasia collision zone, where the crust is thinner. As noted, some have interpreted the adakitic signature as indicating melting of the Tethyan oceanic slab (e.g., Omrani et al., 2008; Khodami et al., 2009; Azizi et al., 2014), versus

fractionation of mantle-derived melts (e.g., Richards et al., 2012), or melting of in-situ or delaminated lower crust (Shafiei et al., 2009; Pang et al., 2016; Lechmann et al., 2018).

In looking more closely at the geochemistry of such suites from Dehaj and across Iran, a common theme appears to be the systematic variation in intra-REE ratios such that each of the suites has a geochemical signature dominated by *either* amphibole or garnet. As already noted, the Dehaj samples appear to have experienced garnet fractionation during magmatic evolution, and this is picked out by the steep trend on a Gd/Dy vs Dy/Yb plot (Figure 11a). However, other suites with amphibole-dominated trends are picked out in narrower ranges of Gd/Dy forming roughly linear arrays relative to Dy/Yb such as the Kerman dataset of Shafiei et al. (2009), given that amphibole has $D_{Dy}<D_{Gd}$ (Davidson et al., 2013). The garnet association is apparent not just at Dehaj, but also Tabriz (Jahangiri, 2007) and Meshkan (Shabanian et al., 2012). A trend more consistent with amphibole involvement is present in the data from different centres in Kerman Province, SE Iran (Shafiei et al., 2009; Zarasvandi et al., 2015). Some datasets are not conclusive, perhaps because several centres are grouped together, as is currently the case for centres near Isfahan (Khodami et al., 2009), or the compositional range is too small to show fractionation trends (Pang et al., 2016). Similar relationships can be determined from the plot of La/Sm v Sm/Yb (Figure 11b). Whereas the Dehaj samples of our study and Pang et al (2016) form an array heading towards high Sm/Yb values (i.e. a garnet signature), other suites from Iran plot in more restricted fields towards the low-Sm/Yb side of the diagram, indicating amphibole control, or possibly a joint amphibole/garnet effect.

5.4. Relationship to mineralization

Of all the adakitic suites described across Iran in recent years, it is notable that whilst a few are clearly linked to economic porphyry copper mineralization (Shafiei et al., 2009; Zarasvandi et al., 2015), most are not (Jahangiri, 2007; Omrani et al., 2008; Khodami et al., 2009; Shabanian et al., 2012; Azizi et al., 2014; Pang et al., 2016; this study). We can now reveal that suites associated with economic mineralization are more *generally* those where amphibole is strongly implicated in the petrogenetic history (Figure 11a, b), specifically some of the centres from the Kerman region, SE Iran (Shafiei et al., 2009; Zarasvandi et al., 2015). Garnet is more clearly involved in the development of centres that do not contain economic deposits (including the Dehaj centre in this study), although Shafiei et al (2009) noted garnet signatures (high Sm/Yb) in just two individual samples from centres with economic deposits. We regard the association of amphibole signatures and mineralization, but not garnet, as robust enough to merit further investigation. The La/Sm v Sm/Yb diagram has previously been used for the study of magmatic rocks associated with copper and gold mineralization in the Central Andes (Figure 11b; Kay and Mpodozis, 2001). Notably few Iranian samples plot within the field associated with copper and/or gold mineralization in the Andes, including suites from economic centres in the Kerman region (Shafiei et al 2009; Zarasvandi et al., 2015).

Why some centres should show amphibole control on MREE and HREE fractionation, and others garnet control, is clearly a subject for further study. Overall crustal thickness is likely to be an important factor in the depth at which magmas crystallise (Kay and Mpodozis, 2001), but unlikely to be a complete explanation, given that economic and non-economic centres exist within the same region of SE Iran, developed at roughly the same time. Although many of the major copper deposits in SE Iran are Middle to Late Miocene age (16-5 Ma), others are Early Miocene, coinciding with barren centres (see age compilations in Shafiei et al., 2009 and Zarasvandi et al., 2015). It may be that there are more local controls on the depths at which magma fractionates, for example the stress conditions at the time

548 of magma transfer from the mantle through the crust (Hutton, 1982) or the extent to which metals are
549 concentrated in the magmas or scavenged from the local crust.
550
551 **6. Conclusions**
552
553 Contemporary igneous rocks from Dehaj, SE Iran, belong to two distinct magmatic series. One
554 series is entirely intrusive and is of high silica adakitic affinity and the second, comprising both
555 hawaiite to trachyandesite lavas and intrusive rocks, is of high-K, non-adakitic affinity. Some rocks are
556 geochemically transitional between the series and are proposed as hybrids formed by magma mixing
557 between the adakitic and high-K series.
558
559 The high-K rocks are derived from melting of subduction-modified lithospheric mantle in the
560 shallowest part of the garnet-spinel transition zone. The chemical signatures and degree of LREE and
561 LILE enrichment are consistent with very small degree partial melting (0.1-1 %), mirroring models for
562 other parts of the Turkish-Iranian Plateau with thick lithosphere (Allen et al., 2013; Sugden et al.,
563 2019). It is determined that the adakitic samples are unrelated to the high-K series and did not
564 experience interaction with mantle wedge peridotite. They are therefore unlikely to be partial melts
565 from a subducted slab at depths greater than that responsible for generation of the high-K series. The
566 adakites have high Sr concentrations, demanding that plagioclase was absent or breaking down during
567 partial melting. Such eclogite-facies conditions might lie at the very base of the crust or as slivers of
568 tectonically delaminated lower crust incorporated in the mantle.
569
570 Within the adakite series, increasing SiO_2 is correlated with markers of adakitic chemistry such
571 as La/Yb and Sr/Y. Garnet fractionation during magma evolution is the key agent for decreasing HREE

ratios, based on intra-REE variations. Garnet fractionation is consistent with the stalling of upwelling magmas in deep seated magma chambers within the thickened crust in this part of the Turkish-Iranian Plateau. We interpret several other late Cenozoic igneous suites from Iran to have involved garnet and/or amphibole during the production of adakite-like signatures, either as a residual or fractionating phase, and suggest that sites of porphyry mineralisation associated with these rocks tend to favour those which involved amphibole and not garnet. As a final note, we caution for care in interpreting the source and evolution of adakitic rocks. As has been observed here, past work has often been biased towards felsic lithologies meaning that contemporary mafic lithologies, which play a critical role in limiting possible adakite origins, may be overlooked.

Acknowledgements

We thank the Geological Survey of Iran for their help in conducting this research. We thank several anonymous referees and David Lentz, for constructive comments. This work was supported by the Natural Environment Research Council, UK (NE/H021620/1) and with internal funding from the Geological Survey of Iran for field studies.

References

Aftabi, A., Atapour, H., 2009. Comments on "Arc magmatism and subduction history beneath the Zagros Mountains, Iran: A new report of adakites and geodynamic consequences" by J. Omrani, P. Agard, H. Whitechurch, M. Bennoit, G. Prouteau, L. Jolivet. Lithos 113, 844-846.

Agard, P., Omrani, J., Jolivet, L., Mouthereau, F., 2005. Convergence history across Zagros (Iran): constraints from collisional and earlier deformation. International Journal of Earth Sciences 94, 401-419.

Agard, P., Omrani, J., Jolivet, L., Whitechurch, H., Vrielynck, B., Spakman, W., Monie, P., Meyer, B., Wortel, R., 2011. Zagros orogeny: a subduction-dominated process. Geological Magazine 148, 692-725.

Allen, M., Jackson, J., Walker, R., 2004. Late Cenozoic reorganization of the Arabia-Eurasia collision and the comparison of short-term and long-term deformation rates. Tectonics 23, TC2008, doi: 2010.1029/2003TC001530.

Allen, M.B., Armstrong, H.A., 2008. Arabia-Eurasia collision and the forcing of mid Cenozoic global cooling. Palaeogeography Palaeoclimatology Palaeoecology 265, 52-58.

Allen, M.B., Kheirkhah, M., Neill, I., Emami, M.H., McLeod, C.L., 2013. Generation of arc and within-plate chemical signatures in collision zone magmatism: Quaternary lavas from Kurdistan Province, Iran. Journal of Petrology 54, 887-911.

Alonso-Perez, R., Muntener, O., Ulmer, P., 2009. Igneous garnet and amphibole fractionation in the roots of island arcs: experimental constraints on andesitic liquids. Contributions to Mineralogy And Petrology 157, 541-558.

Asadi, S., Moore, F., Zarasvandi, A., 2014. Discriminating productive and barren porphyry copper deposits in the southeastern part of the central Iranian volcano-plutonic belt, Kerman region, Iran: A review. Earth-Science Reviews 138, 25-46.

Atherton, M.P., Petford, N., 1993. Generation of sodium-rich magmas from newly underplated basaltic crust. Nature 362, 144-146.

Azizi, H., Asahara, Y., Tsuboi, M., Takemura, K., Razyani, S., 2014. The role of heterogenetic mantle in the genesis of adakites northeast of Sanandaj, northwestern Iran. Chemie Der Erde-Geochemistry 74, 87-97.

Bottrill, A.D., van Hunen, J., Allen, M.B., 2012. Insight into collision zone dynamics from topography: numerical modelling results and observations. Solid Earth 3, 387-399.

Castillo, P.R., 2012. Adakite petrogenesis. Lithos 134, 304-316.

Chen, S., Niu, Y., Li, J., Sun, W., Zhang, Y., Hu, Y., Shao, F., 2016. Syn-collisional adakitic granodiorites formed by fractional crystallization: Insights from their enclosed mafic magmatic enclaves (MMEs) in the Qumushan pluton, North Qilian Orogen at the northern margin of the Tibetan Plateau. Lithos 248, 455-468.

Chiaradia, M., Muntener, O., Beate, B., Fontignie, D., 2009. Adakite-like volcanism of Ecuador: lower crust magmatic evolution and recycling. Contributions to Mineralogy and Petrology 158, 563-588.

Chiu, H.Y., Chung, S.L., Zarrinkoub, M.H., Mohammadi, S.S., Khatib, M.M., Iizuka, Y., 2013. Zircon U-Pb age constraints from Iran on the magmatic evolution related to Neotethyan subduction and Zagros orogeny. Lithos 162-163, 70-87.

644 Chung, S.L., Liu, D.Y., Ji, J.Q., Chu, M.F., Lee, H.Y., Wen, D.J., Lo, C.H., Lee, T.Y., Qian, Q.,
645 Zhang, Q., 2003. Adakites from continental collision zones: Melting of thickened lower crust beneath
646 southern Tibet. Geology 31, 1021-1024.
647
648 Clemens, J.D., Tearron, L.M., Stevens, G. 2006. Barberton (South Africa) TTG magmas: geochemical
649 and experimental constraints on source-rock petrology, pressure of formation and tectonic setting.
650 Precambrian Research 151, 53-78.
651
652 Davidson, J., Turner, S., Plank, T., 2013. Dy/Dy*: Variations Arising from Mantle Sources and
653 Petrogenetic Processes. Journal of Petrology 54, 525-537.
654
655 Deevsalar, R., Shinjo, R., Wang, K.-L., Yeganehfar, H., Neill, I. 2018. Gabbroic-dioritic dykes from
656 the Sanandaj-Sirjan Zone: windows on Jurassic and Eocene geodynamic processes in the Zagros
657 Orogen, Western Iran. Journal of the Geological Society 175, 915-933.
658
659 Deevsalar, R., Shinjo, R., Ghaderi, M., Murata, M., Hoskin, P.W.O., Oshiro, S., Wang, H.-Y., Lee, K.-
660 L., Neill, I. 2017. Mesozoic-Cenozoic mafic magmatism in Sanandaj-Sirjan Zone, Zagros Orogen
661 (western Iran): Geochemical and isotopic inferences from Middle Jurassic and Late Eocene gabbros.
662 Lithos 284, 588-607.
663
664 Defant, M.J., Drummond, M.S., 1990. Derivation of some modern arc magmas by melting of young
665 subducted lithosphere Nature 347, 662-665.
666

667 Defant, M.J., Richerson, P.M., Deboer, J.Z., Stewart, R.H., Maury, R.C., Bellon, H., Drummond, M.S.,
668 Feigenson, M.D., Jackson, T.E., 1991. Dacite genesis via both slab melting and differentiation -
669 petrogenesis of La-Yeguada colcanic complex, Panama. Journal of Petrology 32, 1101-1142.
670
671 Dewey, J.F., Ryan, P.D., Andersen, T.B., 1993. Orogenic uplift and collapse, crustal thickness, fabrics
672 and metamorphic phase changes: the role of eclogites. In: Prichard, H.M., Alabaster, T., Harris,
673 N.B.W., Neary, C.R. (Eds) Magmatic Processes and Plate Tectonics. Geological Society of London
674 Special Publications 76, 325-343.
675
676 Francois, T., Burov, E., Agard, P., Meyer, B., 2014. Buildup of a dynamically supported orogenic
677 plateau: Numerical modeling of the Zagros/Central Iran case study. Geochemistry Geophysics
678 Geosystems 15, 2632-2654.
679
680 Furman, T., Graham, D., 1999. Erosion of lithospheric mantle beneath the East African Rift system:
681 geochemical evidence from the Kivu volcanic province. Lithos 48, 237-262.
682
683 Ghorbani, M.R., Graham, I.T., Ghaderi, M., 2014. Oligocene-Miocene geodynamic evolution of the
684 central part of Urumieh-Dokhtar Arc of Iran. International Geology Review 56, 1039-1050.
685
686 Guan, Q., Zhu, D.-C., Zhao, Z.-D., Dong, G.-C., Zhang, L.-L., Li, X.-W., Liu, M., Mo, X.-X., Liu, Y.-
687 S., Yuan, H.-L., 2012. Crustal thickening prior to 38 Ma in southern Tibet: Evidence from lower crust-
688 derived adakitic magmatism in the Gangdese Batholith. Gondwana Research 21, 88-99.
689

690 Hafkenscheid, E., Wortel, M.J.R., Spakman, W., 2006. Subduction history of the Tethyan region
691 derived from seismic tomography and tectonic reconstructions. Journal of Geophysical Research-Solid
692 Earth 111, B08401, doi:10.1029/2005jb003791.
693
694 Hassanzadeh, Y., Wernicke, B.P. 2016. The Neotethyan Sanandaj-Sirjan zone of Iran as an archetype
695 for passive margin-arc transitions. Tectonics 35, 586-621.
696
697 Hastie, A.R., Kerr, A.C., Pearce, J.A., Mitchell, S.F., 2007. Classification of altered volcanic island arc
698 rocks using immobile trace elements: Development of the Th-Co discrimination diagram. Journal of
699 Petrology 48, 2341-2357.
700
701 Hastie, A.R., Fitton, J.G., Mitchell, S.F., Neill, I., Nowell, G.M., Millar, I.L., 2015. Can fractional
702 crystallization, mixing and assimilation processes be responsible for Jamaican-type adakites?
703 Implications for generating Eoarchaean continental crust. Journal of Petrology 56, 1251-1283.
704
705 Hutton, D.H.W., 1982. A tectonic model for the emplacement of the Main Donegal Granite, NW
706 Ireland. Journal of the Geological Society 139, 615-631.
707
708 Jackson, J., 1992. Partitioning of strike-slip and convergent motion between Eurasia and Arabia in
709 eastern Turkey and the Caucasus. Journal of Geophysical Research 97, 12471-12479.
710
711 Jahangiri, A., 2007. Post-collisional Miocene adakitic volcanism in NW Iran: Geochemical and
712 geodynamic implications. Journal of Asian Earth Sciences 30, 433-447.
713

714 Kaislaniemi, L., van Hunen, J., Allen, M.B., Neill, I., 2014. Sublithospheric small-scale convection-A
715 mechanism for collision zone magmatism. Geology 42, 291-294.
716
717 Karakhanian, A., Djrbashian, R., Trifonov, V., Philip, H., Arakelian, S., Avagian, A. 2002. Holocene-
718 historical volcanism and active faults as natural risk factors for Armenia and adjacent countries. Journal
719 of Volcanology and Geothermal Research 113, 319-344.
720
721 Kay, S.M., Maksaev, V., Moscoso, R., Mpodozis, C., Nasi, C., 1987. Probing the evolving Andean
722 lithosphere - Mid-late Tertiary magmatism in Chile (29-degrees-30-degrees-30'S) over the modern
723 zone of subhorizontal subduction. Journal of Geophysical Research-Solid Earth and Planets 92, 6173-
724 6189.
725
726 Kay, S.M., Mpodozis, C., 2001. Central Andean ore deposits linked to evolving shallow subduction
727 systems and thickening crust. GSA Today 11, 4-9.
728
729 Keskin, M., 2003. Magma generation by slab steepening and breakoff beneath a subduction-accretion
730 complex: An alternative model for collision-related volcanism in Eastern Anatolia, Turkey.
731 Geophysical Research Letters 30, 1-4.
732
733 Keskin, M., Pearce, J.A., Mitchell, J.G., 1998. Volcano-stratigraphy and geochemistry of collision-
734 related volcanism on the Erzurum-Kars Plateau, northeastern Turkey. Journal of Volcanology and
735 Geothermal Research 85, 355-404.
736

737 Kheirkhah, M., Allen, M.B., Emami, M., 2009. Quaternary syn-collision magmatism from the
738 Iran/Turkey borderlands. Journal of Volcanology and Geothermal Research 182, 1-12.
739
740 Kheirkhah, M., Neill, I., Allen, M.B., 2015. Petrogenesis of OIB-like basaltic volcanic rocks in a
741 continental collision zone: Late Cenozoic magmatism of Eastern Iran. Journal of Asian Earth Sciences
742 106, 19-33.
743
744 Kheirkhah, M., Neill, I., Allen, M.B., Ajdari, K., 2013. Small-volume melts of lithospheric mantle
745 during continental collision: Late Cenozoic lavas of Mahabad, NW Iran. Journal of Asian Earth
746 Sciences 74, 37-49.
747
748 Khodami, M., Noghreyan, M., Davoudian, A.R., 2009. Pliocene-Quaternary adakite volcanism in the
749 Isfahan area, Central Iranian magmatic belt. Neues Jahrbuch Fur Mineralogie-Abhandlungen 186, 235-
750 248.
751
752 Lechmann, A., Burg, J.-P., Ulmer, P., Guillong, M., Faridi, M. 2018. Metsomatised mantle as the
753 source of Mid-Miocene-Quaternary volcanism in NW-Iranian Azerbaijan: geochronological and
754 geochemical evidence. Lithos 304, 311-328.
755
756 Li, J.X., Qin, K.Z., Li, G.M., Xiao, B., Chen, L., Zhao, J.X., 2011. Post-collisional ore-bearing adakitic
757 porphyries from Gangdese porphyry copper belt, southern Tibet: Melting of thickened juvenile arc
758 lower crust. Lithos 126, 265-277.
759

760 Macpherson, C.G., Dreher, S.T., Thirlwall, M.F., 2006. Adakites without slab melting: High pressure
761 differentiation of island arc magma, Mindanao, the Philippines. Earth and Planetary Science Letters
762 243, 581-593.
763
764 Maggi, A., Priestley, K., 2005. Surface waveform tomography of the Turkish-Iranian plateau.
765 Geophysical Journal International 160, 1068-1080.
766
767 Magni, V., Allen, M.B., van Hunen, J, Bouilhol, P., 2017. Continental underplating after slab break-off.
768 Earth and Planetary Science Letters 474, 59-67.
769
770 Martin, H., 1999. Adakitic magmas: modern analogues of Archaean granitoids. Lithos 46, 411-429.
771 Mahood, G., Hildreth, W., 1983. Large partition-coefficients for trace elements in high-silica rhyolites
772 Geochimica Et Cosmochimica Acta 47, 11-30.
773
774 Martin, H., Smithies, R.H., Rapp, R., Moyen, J.F., Champion, D., 2005. An overview of adakite,
775 tonalite-trondhjemite-granodiorite (TTG), and sanukitoid: relationships and some implications for
776 crustal evolution. Lithos 79, 1-24.
777
778 McDonough, W.F., Sun, S.S., 1995. The composition of the Earth. Chemical Geology 120, 223-253.
779
780 McQuarrie, N., van Hinsbergen, D.J.J., 2013. Retrodeforming the Arabia-Eurasia collision zone: Age
781 of collision versus magnitude of continental subduction. Geology 41, 315-318.
782

Mortazavi, M., Sparks, R.S.J., Amigo, A., 2009. Evidence for recent large magnitude explosive eruptions at Damavand volcano, Iran, with implications for volcanic hazards. Journal of Sciences, Islamic Republic of Iran 20, 253-264.

Moyen, J.-F., 2009. High Sr/Y and La/Yb ratios: the meaning of the "adakitic signature". Lithos 112, 556-574.

Neill, I., Meliksetian, K., Allen, M.B., Navarsardyan, G., Karapetyan, S., 2013. Pliocene-Quaternary volcanic rocks of NW Armenia: Magmatism and lithospheric dynamics within an active orogenic plateau. Lithos 180, 200-215.

Neill, I., Meliksetian, K., Allen, M.B., Navasardyan, G., Kuiper, K., 2015. Petrogenesis of mafic collision zone magmatism: The Armenian sector of the Turkish-Iranian Plateau. Chemical Geology 403, 24-41.

Omrani, J., Agard, P., Whitechurch, H., Benoit, M., Prouteau, G., Jolivet, L., 2008. Arc-magmatism and subduction history beneath the Zagros Mountains, Iran: A new report of adakites and geodynamic consequences. Lithos 106, 380-398.

Pang, K.N., Chung, S.L., Zarrinkoub, M.H., Li, X.H., Lee, H.Y., Lin, T.H., Chiu, H.Y., 2016. New age and geochemical constraints on the origin of Quaternary adakite-like lavas in the Arabia Eurasia collision zone. Lithos 264, 348-359.

Pang, K.N., Chung, S.L., Zarrinkoub, M.H., Mohammadi, S.S., Yang, H.M., Chu, C.H., Lee, H.Y., Lo, C.H., 2012. Age, geochemical characteristics and petrogenesis of Late Cenozoic intraplate alkali basalts in the Lut-Sistan region, eastern Iran. Chemical Geology 306, 40-53.

Pe-Piper, G., Piper, D.J.W., 2001. Late Cenozoic, post-collisional Aegean igneous rocks: Nd, Pb and Sr isotopic constraints on petrogenetic and tectonic models. Geological Magazine 138, 653-668.

Peacock, S.M., Rushmer, T., Thompson, A.B., 1994. Partial melting of subducted oceanic crust. Earth and Planetary Science Letters 121, 227-244.

Pearce, J.A., 1983. Role of the sub-continental lithosphere in magma genesis at active continental margins. In: Hawkesworth, C.J., Norry, M.J. (Eds) Continental Basalts and Mantle Xenoliths. Natwich, Shiva Press, 230-249.

Pearce, J.A., Bender, J.F., Delong, S.E., Kidd, W.S.F., Low, P.J., Guner, Y., Sargolu, F., Yilmaz, Y., Moorbath, S., Mitchell, J.G., 1990. Genesis of collision volcanism in eastern Anatolia, Turkey. Journal of Volcanology and Geothermal Research 44, 189-229.

Peccerillo, A., Taylor, S.R., 1976. Geochemistry of Eocene calc-alkaline volcanic rocks from Kastamonu area, northern Turkey. Contributions to Mineralogy and Petrology 58, 63-81.

Priestley, K., McKenzie, D., Barron, J., Tatar, M., Debayle, E., 2012. The Zagros core: Deformation of the continental lithospheric mantle. Geochemistry Geophysics Geosystems 13, doi: 10.1029/2012gc004435.

Reuter, M., Piller, W.E., Harzhauser, M., Mandic, O., Berning, B., Rogl, F., Kroh, A., Aubry, M.P., Wielandt-Schuster, U., Hamedani, A., 2009. The Oligo-/Miocene Qom Formation (Iran): evidence for an early Burdigalian restriction of the Tethyan Seaway and closure of its Iranian gateways. International Journal of Earth Sciences 98, 627-650.

Richards, J.P., 2011. High Sr/Y arc magmas and porphyry Cu +/- Mo +/- Au deposits: just add water. Economic Geology 106, 1075-1081.

Richards, J.P., Spell, T., Rameh, E., Razique, A., Fletcher, T., 2012. High Sr/Y Magmas Reflect Arc Maturity, High Magmatic Water Content, and Porphyry Cu +/- Mo +/- Au Potential: Examples from the Tethyan Arcs of Central and Eastern Iran and Western Pakistan. Economic Geology 107, 295-332.

Richards, J.P., Wilkinson, D., Ullrich, T., 2006. Geology of the Sari Gunay epithermal gold deposit, northwest Iran. Economic Geology 101, 1455-1496.

Richards, J.R., Kerrich, R., 2007. Special paper: Adakite-like rocks: Their diverse origins and questionable role in metallogenesis. Economic Geology 102, 537-576.

Rodriguez, C., Selles, D., Dungan, M., Langmuir, C., Leeman, W., 2007. Adakitic dacites formed by intracrustal crystal fractionation of water-rich parent magmas at Nevado de Longav volcano (36.2 degrees S; Andean Southern Volcanic Zone, central Chile). Journal of Petrology 48, 2033-2061.

Rooney, T.O., Franceschi, P., Hall, C.M., 2011. Water-saturated magmas in the Panama Canal region: a precursor to adakite-like magma generation? Contributions to Mineralogy and Petrology 161, 373-388.

Saadat, S., Stern, C.R., 2012. Petrochemistry of a xenolith-bearing Neogene alkali olivine basalt from northeastern Iran. Journal of Volcanology and Geothermal Research 225, 13-29.

Seber, D., Sandvol, E., Sandvol, C., Brindisi, C., Barazangi, M., 2001. Crustal model for the Middle East and North Africa region: implications for the isostatic compensation mechanism. Geophysical Journal International 147, 630-638.

Şengör, A.M.C., Altiner, D., Cin, A., Ustaomer, T., Hsu, K.J. 1988. Origin and assembly of the Tethyside orogenic collage at the expense of Gondwana Land. In: Audley-Charles, M.G. and Hallam, A. (Eds). Gondwana and Tethys. Geological Society of London Special Publications 37, 119-181.

Seyedrahimi-Niaraq, M., Ardejani, F.D., Noorollahi, Y., Porkhial, S. 2017. Development of an updated geothermal reservoir conceptual model for NW Sabalan geothermal field, Iran. Geothermal Energy 5, 14.

Shabanian, E., Acocella, V., Gioncada, A., Ghasemi, H., Bellier, O., 2012. Structural control on volcanism in intraplate post collisional settings: Late Cenozoic to Quaternary examples of Iran and Eastern Turkey. Tectonics 31, doi: 10.1029/2011tc003042.

874 Shafiei, B., Haschke, M., Shahabpour, J., 2009. Recycling of orogenic arc crust triggers porphyry Cu
875 mineralization in Kerman Cenozoic arc rocks, southeastern Iran. Mineralium Deposita 44, 265-283.
876
877 Shaker Ardakani, A., 2016. Post-collisional Plio-Pleistocene Anar-Dehaj adakitic subvolcanic domes in
878 the central volcanic belt of Iran: geochemical characteristics and tectonic implications. Periodico di
879 Mineralogica, 85, 185-200.
880
881 Smithies, R.H., Champion, D.C., van Kranendonk, M.J., 2009. Formation of Paleoarchean continental
882 crust through infracrustal melting of enriched basalt. Earth and Planetary Science Letters 281, 293-306.
883
884 Soheili, M., 1981. Anar. Geological Survey of Iran, Tehran.
885
886 Sugden, P.J., Savov, I.P., Wilson, M., Meliksetian, K., Navasardyan, G., Halama, R. 2019. The
887 thickness of the mantle lithosphere and collision-related volcanism in the Lesser Caucasus. Journal of
888 Petrology 60, 199-230.
889
890 Sun, S.S., McDonough, W.F., 1989. Chemical and isotopic systematics of oceanic basalts: implications
891 for mantle composition and processes, in: Saunders, A.D., Norry, M.J. (Eds.), Magmatism in the Ocean
892 Basins. Geological Society of London Special Publication, pp. 313-345.
893
894 Taghizadeh-Farimand, F., Afsari, N., Sodoudi, F., 2015. Crustal thickness of Iran inferred from
895 converted waves. Pure and Applied Geophysics 172, 309-331.
896

Tiepolo, M., Tribuzio, R., Vannucci, R., 2002. The compositions of mantle-derived melts developed during the Alpine continental collision. Contributions to Mineralogy and Petrology 144, 1-15.

van der Meer, D.G., van Hinsbergen, D.J.J., Spakman, W., 2018. Atlas of the Underworld: slab remnants in the mantle, their sinking history, and a new outlook on lower mantle viscosity. Tectonophysics 723, 309-448.

van Hunen, J., Allen, M.B., 2011. Continental collision and slab break-off: A comparison of 3-D numerical models with observations. Earth and Planetary Science Letters 302, 27-37.

Verdel, C., Wernicke, B.P., Hassanzadeh, J., Guest, B. 2011. A Palaeogene extensional arc flare-up in Iran. Tectonics 30, doi:10.1029/2010TC002809.

Vernant, P., Nilforoushan, F., Hatzfeld, D., Abbassi, M., Vigny, C., Masson, F., Nankali, H., Martinod, J., Ashtiani, A., Bayer, R., Tavakoli, F., Chery, J., 2004. Contemporary crustal deformation and plate kinematics in Middle East constrained by GPS measurements in Iran and northern Iran. Geophysical Journal International 157, 381-398.

Xu, W.C., Zhang, H.F., Luo, B.J., Guo, L., Yang, H., 2015. Adakite-like geochemical signature produced by amphibole-dominated fractionation of arc magmas: An example from the Late Cretaceous magmatism in Gangdese belt, south Tibet. Lithos 232, 197-210.

Zamboni, D., Gazel, E., Ryan, J.G., Cannatelli, C., Lucchi, F., Atlas, Z.D., Trela, J., Mazza, S.E., De Vivo, B. 2016. Contrasting sediment melt and fluid signatures for magma components in the Aeolian

Arc: Implications for numerical modelling of subduction systems. Geochemistry, Geophysics, Geosystems 17, 2034-2053.

Zarasvandi, A., Rezaei, M., Sadeghi, M., Lentz, D., Adelpour, M., Pourkaseb, H., 2015. Rare earth element signatures of economic and sub-economic porphyry copper systems in Urumieh-Dokhtar Magmatic Arc (UDMA), Iran. Ore Geology Reviews 70, 407-423.

Zor, E., Sandvol, E., Gürbüz, C., Türkelli, N., Seber, D., Barazangi, M., 2003. The crustal structure of the East Anatolian plateau from receiver functions. Geophysical Research Letters 30, 8044, doi:8010.1029/2003GL018192.

Figure captions

Figure 1. Location map for Late Cenozoic magmatism on the Turkish-Iranian Plateau. After Kaislaniemi et al. (2014).

Figure 2. (a) Geology of the Dehaj region, adapted from the 1:250,000 Anar map (Soheili, 1981) and overlain with the main sampling locations for mafic lavas and dome samples. (b) satellite imagery from https://earth.google.com (accessed 05/08/2019), showing the relationship between the older Mesozoic to Cenozoic magmatic rocks and the two main Quaternary adakitic domes and mafic lavas.

Figure 3. Field photos of volcanic centres in the Dehaj region. a) DJ1-1, one of the mafic, high-K series lava flows; b) heavily jointed intermediate lava flow DJ2-1 of the transitional samples; c) DJ25-3 in the foreground, another high-K series mafic lava flow, with the mountain Kuh-e-Aj-Bala in the

background, a large stock or dome of the adakite series. See text for full details of the different magmatic series.

Figure 4. Petrography of the newly analysed samples, all with 4 mm horizontal field of view in cross-polarised light. a) DJ1-1 (high-K series) showing groundmass with clinopyroxene phenocrysts, plagioclase and oxides with rare iddingsite replacing olivine. b) DJ2-1 (transitional series) showing a 1 mm glomerocryst of clinopyroxene set in a very fine groundmass. c) DJ5-1 (adakite series) showing a seriate texture dominated by plagioclase, often zoned but not sieve-textured, e.g., the crystal in the centre of the image.

Figure 5. Geochemical discrimination and Harker plots for the Dehaj samples, including previous analyses by Shaker Ardakani (2016) and Pang et al. (2016). a) Total alkalis vs SiO_2. b) K_2O vs SiO_2 after Peccerillo & Taylor (1976). c) Th-Co for immobile elements after Hastie et al. (2007) demonstrating the two main series proposed on (b) are valid. d-g) Harker plots demonstrating compatible behaviour of MgO, Ni and Cr, Sr and Y and incompatible behaviour of Rb. Three high-K lavas with Sr concentrations >3000 ppm have been omitted from (f).

Figure 6. Adakite vs typical arc rock discrimination diagrams from Moyen (2009) alongside ratio-silica Harker plots for adakite-discriminating trace elements, with samples from this work plus Shaker Ardakani (2016) and Pang et al. (2016). a) Sr/Y vs Y. b) Sr/Y vs SiO_2. Having identified the adakitic/medium-K and non-adakitic/high-K series on earlier diagrams, the next two diagrams merge data sources and consistently use this new distinction. c) La/Yb_{CN} vs Yb_{CN} (CN = chondrite-normalised). d) La/Yb_{CN} vs SiO_2. The cut-offs for Sr/Y and La/Yb are from Defant and Drummond (1990), based on Sr/Y and La/Yb (not CN) = 40 and 20, respectively.

968

969 *Figure 7. Multi-element plots for Dehaj incorporating this work plus Shaker Ardakani (2016) and*
970 *Pang et al. (2016). a) Chondrite-normalised REE plot showing all three series. b-d) Primitive mantle-*
971 *normalised spider diagrams, showing b) the high-K series compared with the average adakite; c) the*
972 *adakite/medium-K series with the average high-K series sample; d) the transitional samples showing*
973 *the other series averages for comparison.*

974

975 *Figure 8. Isotopic composition of the two series, including samples analysed for this study, Pang et al.*
976 *(2016) and Omrani et al. (2008). No transitional samples were analysed. As in previous diagrams, the*
977 *adakite series is represented by black squares, and the high-K series by open circles. See the named*
978 *papers on the diagram for comparative data sources.*

979

980 *Figure 9. a) Dy/Dy* diagram after Davidson et al. (2013) showing the enriched nature of the*
981 *source/low volume melting required to form the high-K series (circles), versus the very strong apparent*
982 *garnet control on the REE systematics of the adakite series (squares). The inset shows no relationship*
983 *between Dy/Yb and magmatic evolution for the high-K series, but there is a stronger relationship for*
984 *the adakites. b) Comparison of the high-K series with melt models for amphibole-bearing garnet and*
985 *spinel peridotite for Armenia by Sugden et al. (2019). Syunik in S Armenia represents melting within*
986 *thick lithosphere during amphibole peridotite breakdown, within the garnet-spinel transition zone;*
987 *melting in Shirak in N Armenia is typical of the more voluminous melting at shallow depths across*
988 *much of the Caucasus and E Anatolia.*

989

990 *Figure 10. a) Th/Yb vs Ta/Yb from Pearce (1983) showing the subduction-related geochemical*
991 *signature of the high-K series, with the inset demonstrating little relationship between Th/Yb and*

magmatic evolution. b) Rb/Sr vs Ba/Rb from Furman & Graham (1999) showing a strong residual amphibole control on the high-K series. c) Th/Nb vs La/Nb and d) Th/Nb vs Ba/Nb plots from Zamboni et al. (2016) are used to explore the nature of the past subduction-related materials which contributed to the mantle source of the high-K series, implying a combination of slab-related melts and fluids were responsible.

Figure 11. a) Gy/Yb vs Dy/Yb diagram designed to separate the steep trends related to intra-HREE fractionation caused by amphibole at source or amphibole fractionation, versus garnet. b) La/Sm vs. Sm/Yb to more clearly highlight the role of amphibole at source or during fractionation. Data sources are given on the figure.

Table captions

Table 1. Major and trace element data for the studied rocks from Dehaj, SE Iran. HK = high K series. Transit' = transitional, i.e. samples which fall between the high K and adakite series on various Harker plots and are interpreted to have formed by mixing between the two series. Adakite = meets the definition of high silica adakite (Martin and Moyen, 2003). b.d. = below detection.

Table 2. Sr and Nd isotope data for the studied rocks from Dehaj, SE Iran. Values are normalised to NBS987 $^{87}Sr/^{86}Sr = 0.710240$ and J&M $^{143}Nd/^{144}Nd = 0.511110$ and are not age corrected.

Figure 1

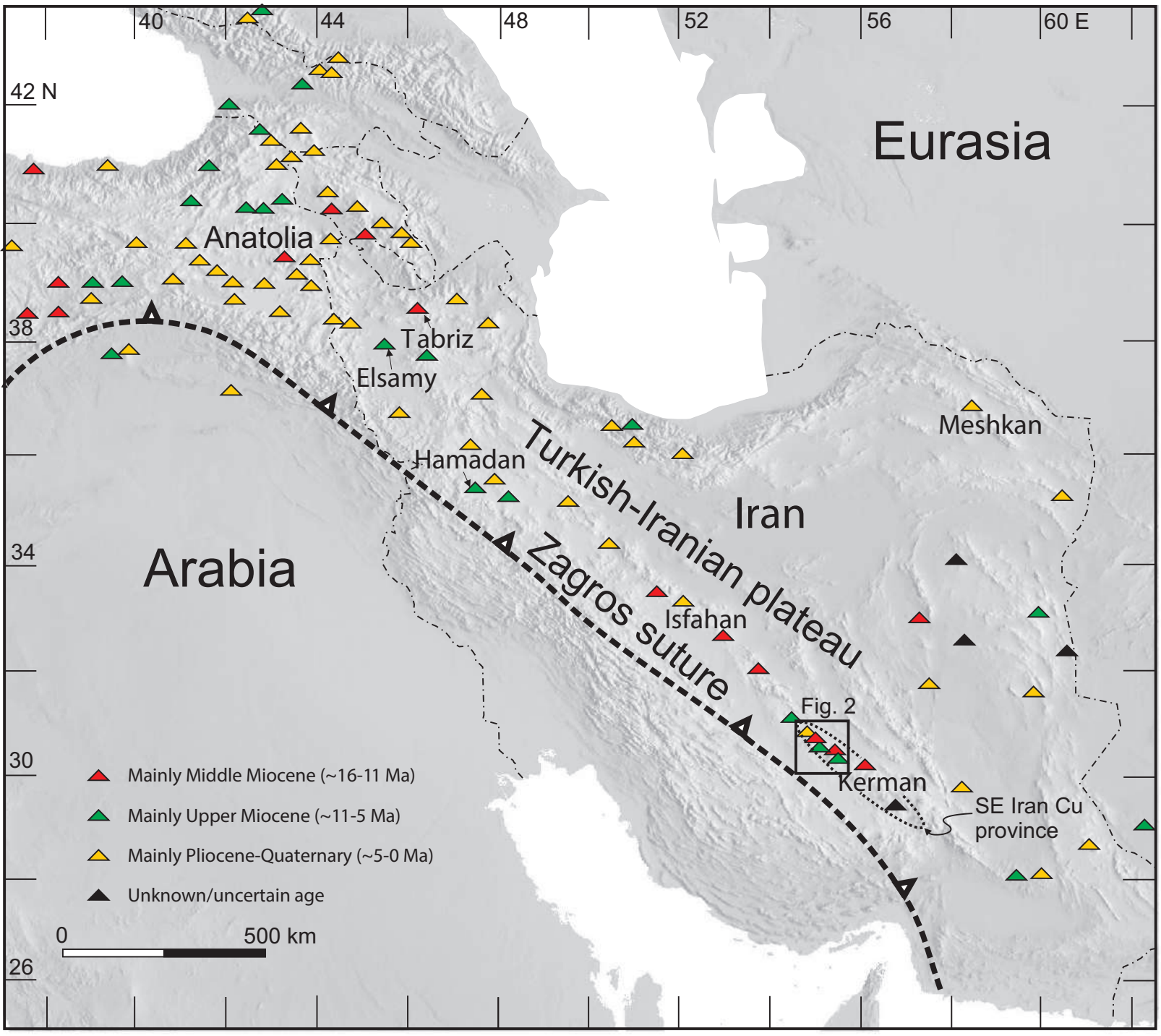
40
44
48
52
56
60 E
42 N
38
34
30
26
Eurasia
Anatolia
Tabriz
Elsamy
Hamadan
Meshkan
Iran
Arabia
Isfahan
Turkish-Iranian plateau
Zagros suture
Fig. 2
Kerman
SE Iran Cu province
Mainly Middle Miocene (~16-11 Ma)
Mainly Upper Miocene (~11-5 Ma)
Mainly Pliocene-Quaternary (~5-0 Ma)
Unknown/uncertain age
0
500 km

Figure 2

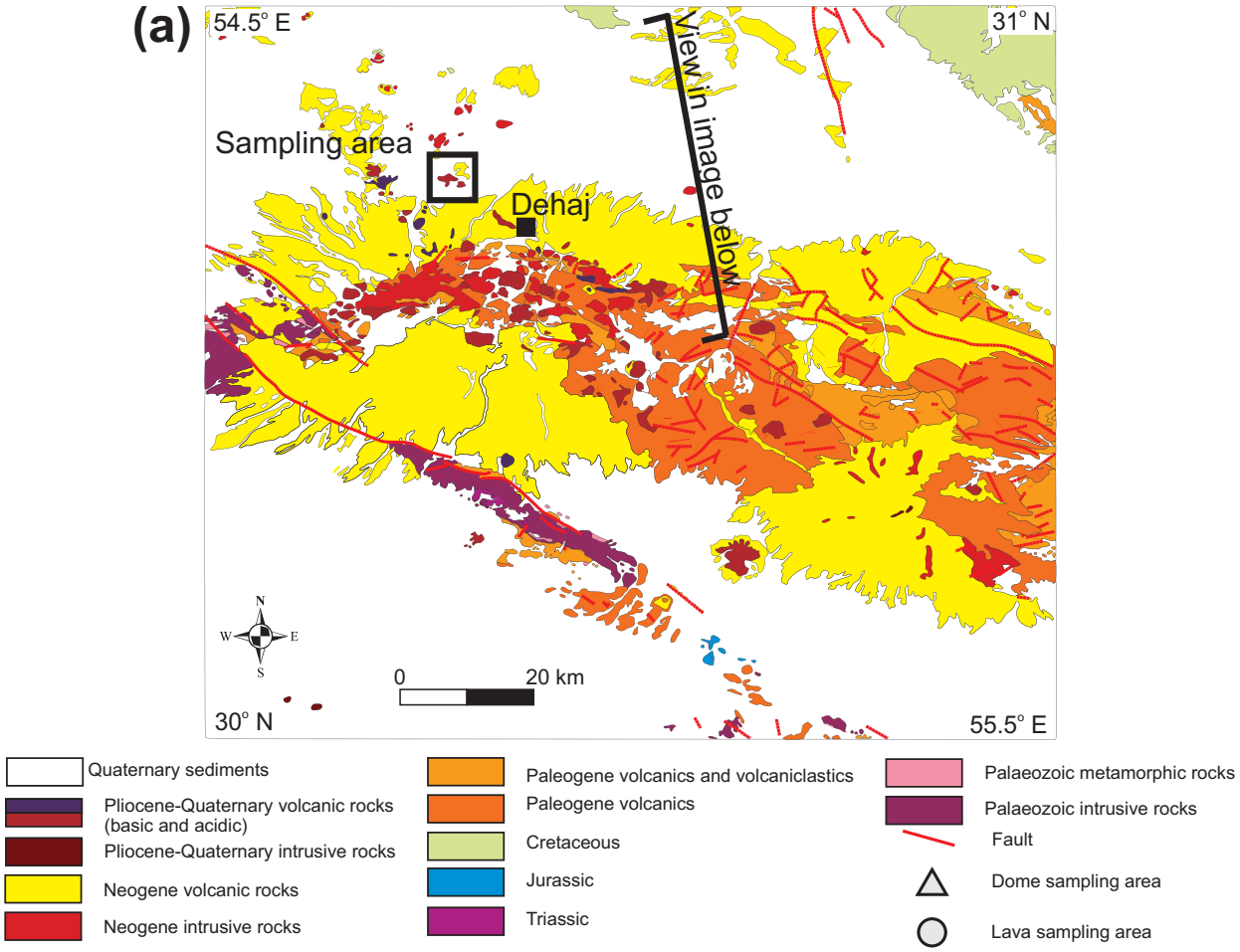
(a)
54.5° E
31° N
Sampling area
Dehaj
View in image below
N
W
E
S
0
20 km
30° N
55.5° E
Quaternary sediments
Pliocene-Quaternary volcanic rocks (basic and acidic)
Pliocene-Quaternary intrusive rocks
Neogene volcanic rocks
Neogene intrusive rocks
Paleogene volcanics and volcaniclastics
Paleogene volcanics
Cretaceous
Jurassic
Triassic
Palaeozoic metamorphic rocks
Palaeozoic intrusive rocks
Fault
Dome sampling area
Lava sampling area

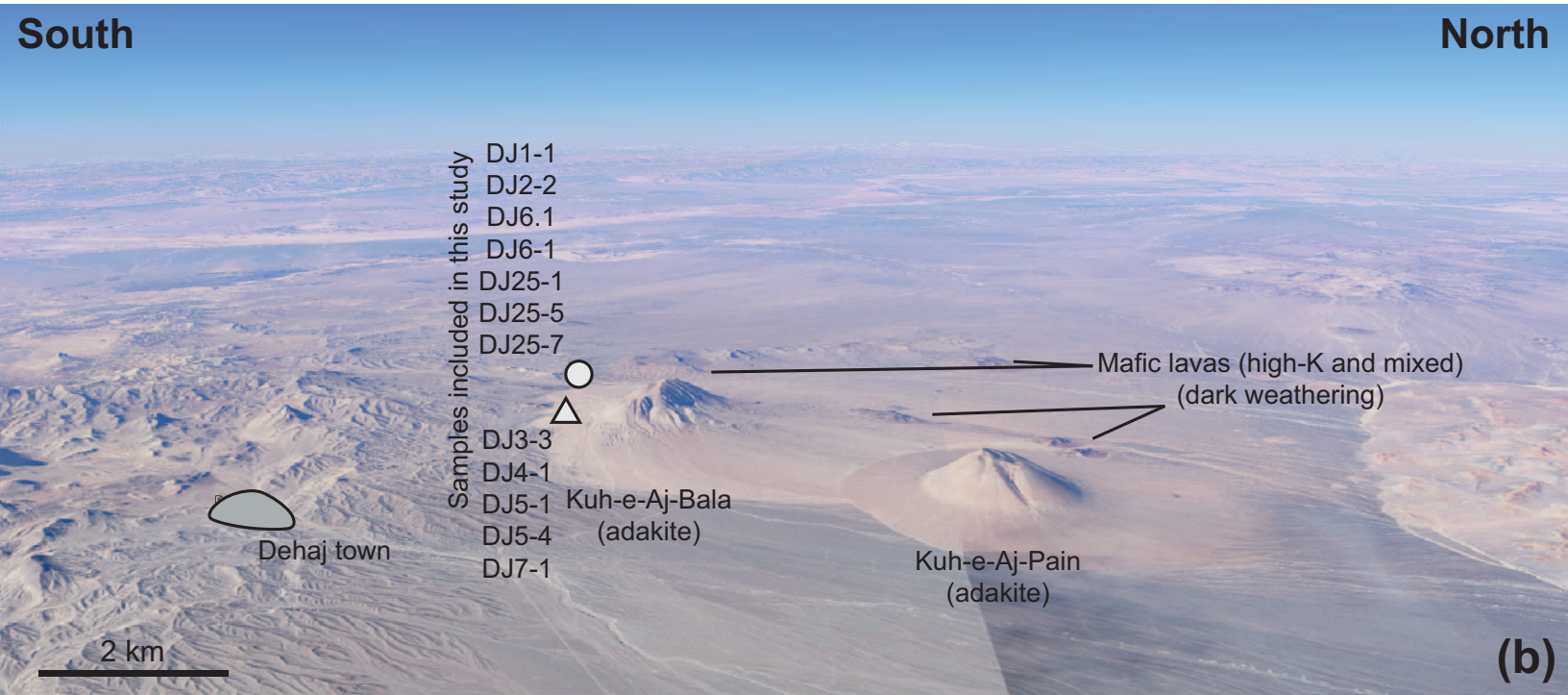
South
North
Samples included in this study
DJ1-1
DJ2-2
DJ6.1
DJ6-1
DJ25-1
DJ25-5
DJ25-7
DJ3-3
DJ4-1
DJ5-1
DJ5-4
DJ7-1
Mafic lavas (high-K and mixed)
(dark weathering)
Kuh-e-Aj-Bala
(adakite)
Dehaj town
Kuh-e-Aj-Pain
(adakite)
2 km
(b)

Figure 3

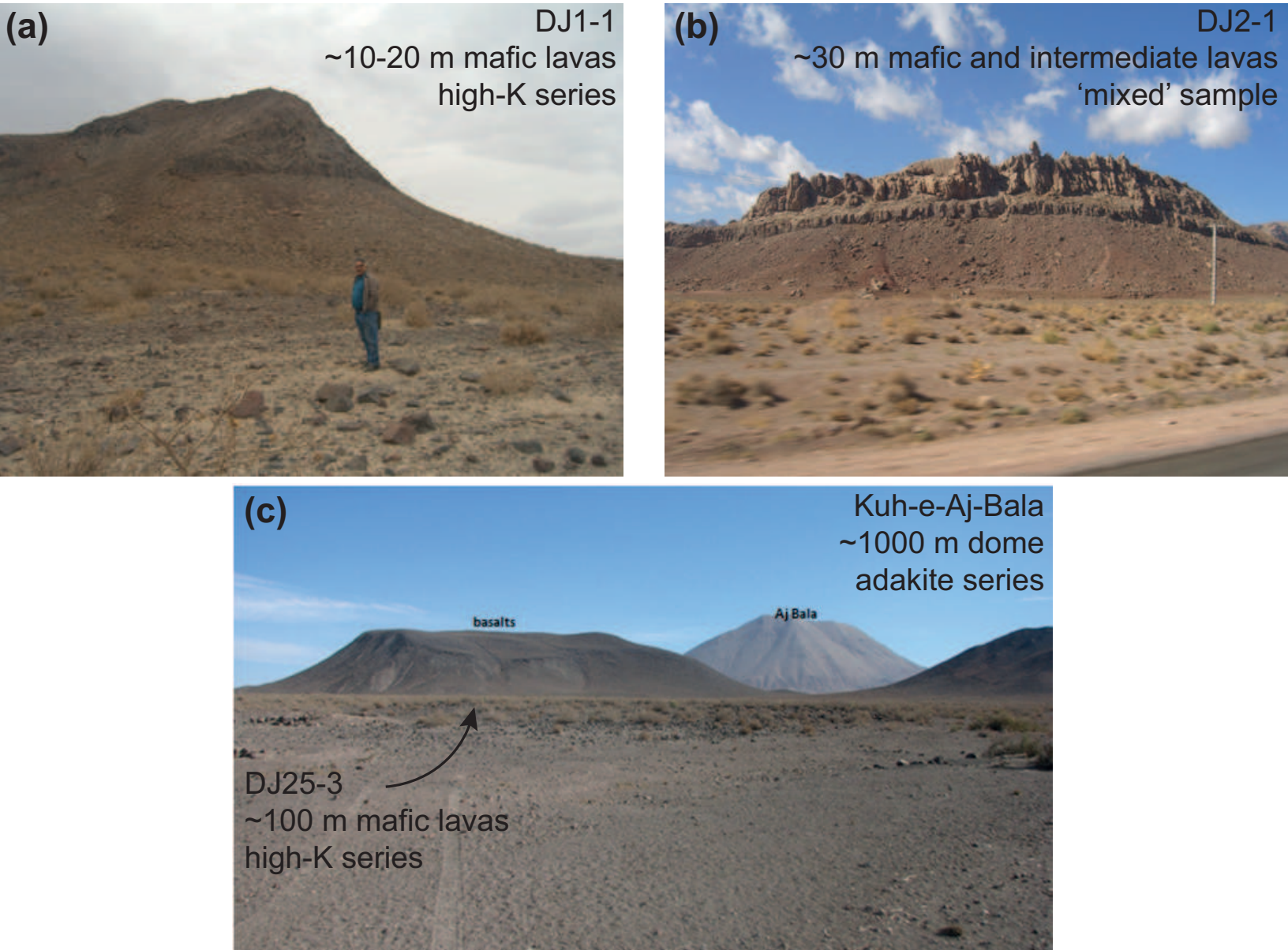
(a)
DJ1-1
~10-20 m mafic lavas
high-K series
(b)
DJ2-1
~30 m mafic and intermediate lavas
'mixed' sample
(c)
Kuh-e-Aj-Bala
~1000 m dome
adakite series
basalts
Aj Bala
DJ25-3
~100 m mafic lavas
high-K series

Figure 4

a
Pl
Cpx
Id (after Ol)
b
Cpx-rich glomerocryst
Pl microlites
c
Pl (weakly sieve-textured)
Pl (zoned)

Figure 5

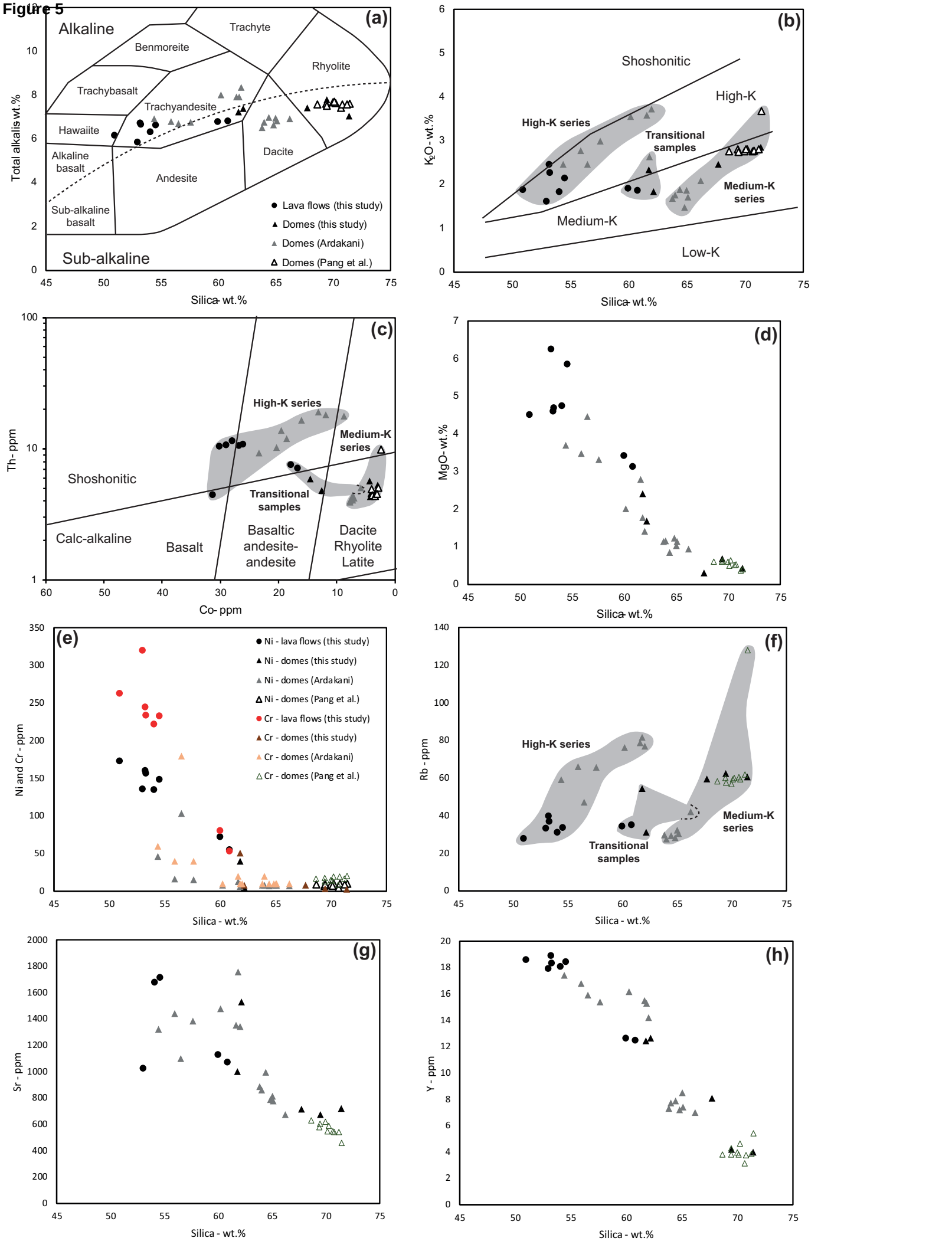
(a)
Alkaline
Trachyte
Benmoreite
Rhyolite
Trachybasalt
Trachyandesite
Hawaiite
Dacite
Alkaline basalt
Andesite
Sub-alkaline basalt
Sub-alkaline
Lava flows (this study)
Domes (this study)
Domes (Ardakani)
Domes (Pang et al.)
Total alkalis wt.%
Silica wt.%
(b)
Shoshonitic
High-K
High-K series
Transitional samples
Medium-K series
Medium-K
Low-K
K2O - wt.%
Silica wt.%
(c)
High-K series
Medium-K series
Shoshonitic
Transitional samples
Calc-alkaline
Basalt
Basaltic andesite-andesite
Dacite Rhyolite Latite
Th - ppm
Co - ppm
(d)
MgO - wt.%
Silica wt.%
(e)
Ni - lava flows (this study)
Ni - domes (this study)
Ni - domes (Ardakani)
Ni - domes (Pang et al.)
Cr - lava flows (this study)
Cr - domes (this study)
Cr - domes (Ardakani)
Cr - domes (Pang et al.)
Ni and Cr - ppm
Silica - wt.%
(f)
High-K series
Medium-K series
Transitional samples
Rb - ppm
Silica - wt.%
(g)
Sr - ppm
Silica - wt.%
(h)
Y - ppm
Silica - wt.%

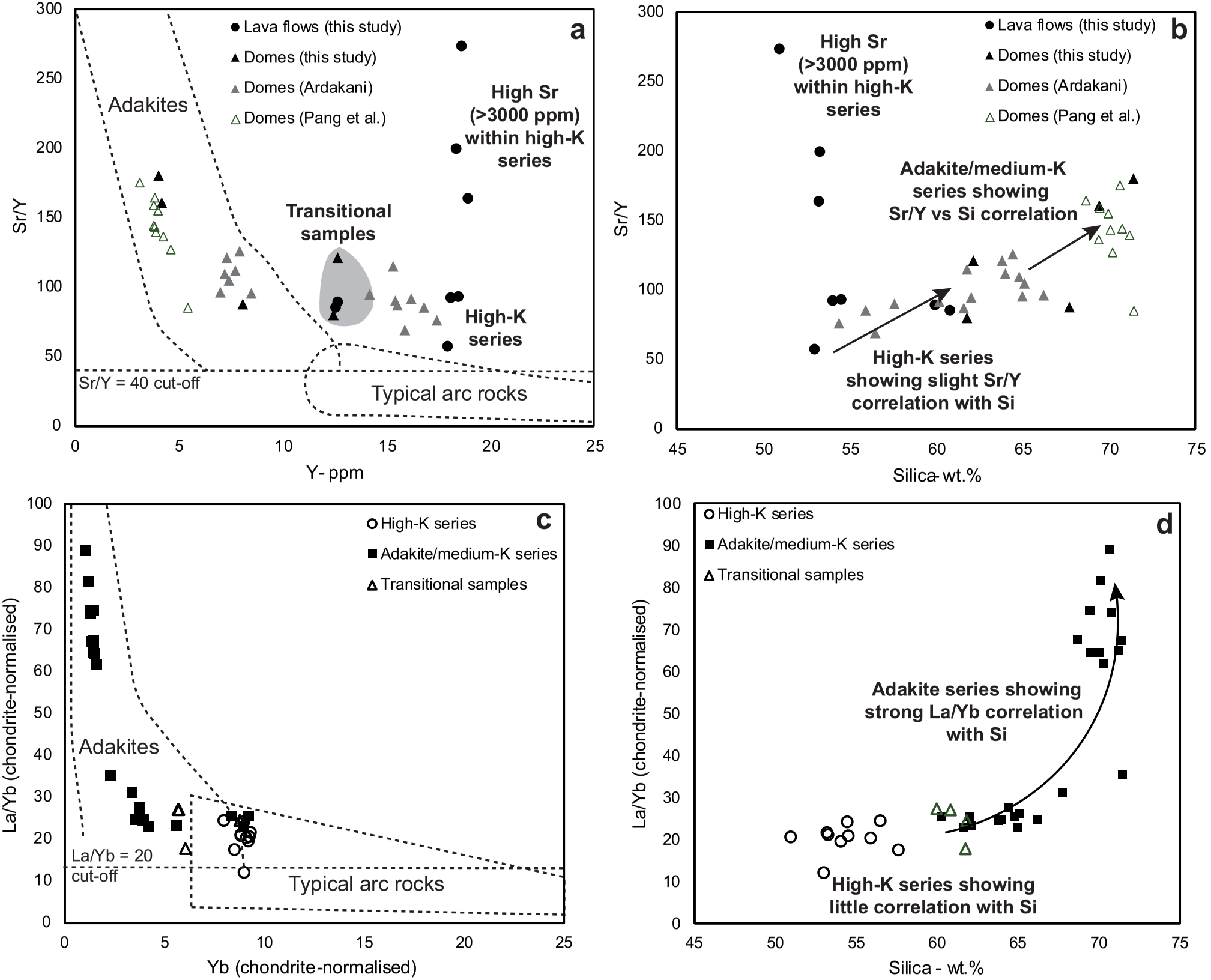
a
Lava flows (this study)
Domes (this study)
Domes (Ardakani)
Domes (Pang et al.)
Adakites
High Sr (>3000 ppm) within high-K series
Transitional samples
High-K series
Sr/Y = 40 cut-off
Typical arc rocks
Sr/Y
Y- ppm
b
High Sr (>3000 ppm) within high-K series
Adakite/medium-K series showing Sr/Y vs Si correlation
High-K series showing slight Sr/Y correlation with Si
Silica- wt.%
c
High-K series
Adakite/medium-K series
Transitional samples
Adakites
La/Yb = 20 cut-off
Typical arc rocks
La/Yb (chondrite-normalised)
Yb (chondrite-normalised)
d
Adakite series showing strong La/Yb correlation with Si
High-K series showing little correlation with Si
Silica - wt.%

Figure 6

Figure 7

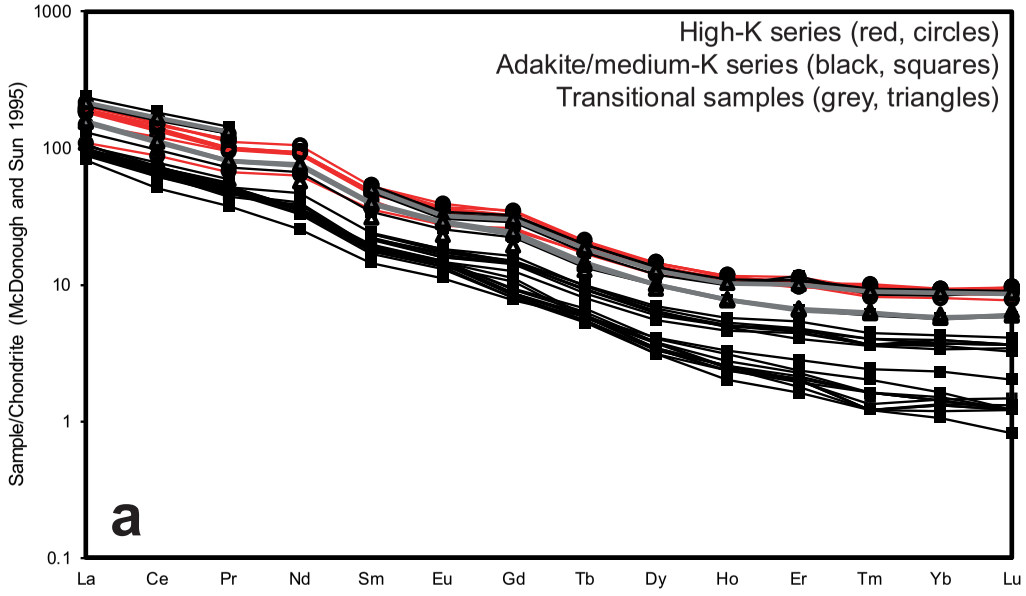
High-K series (red, circles)
Adakite/medium-K series (black, squares)
Transitional samples (grey, triangles)
Sample/Chondrite (McDonough and Sun 1995)
1000
100
10
1
0.1
a
La Ce Pr Nd Sm Eu Gd Tb Dy Ho Er Tm Yb Lu

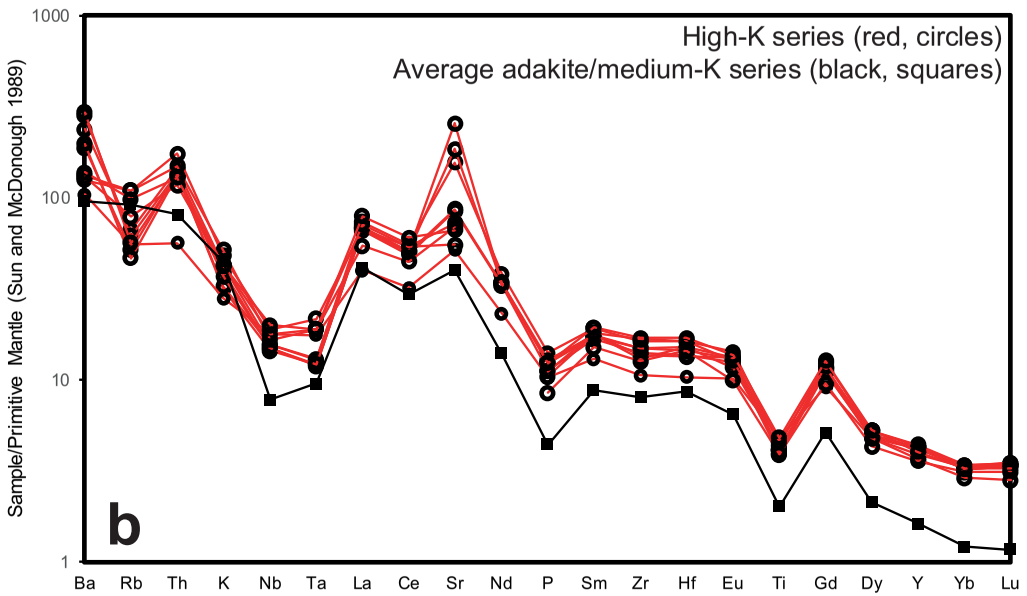
High-K series (red, circles)
Average adakite/medium-K series (black, squares)
Sample/Primitive Mantle (Sun and McDonough 1989)
1000
100
10
1
b
Ba Rb Th K Nb Ta La Ce Sr Nd P Sm Zr Hf Eu Ti Gd Dy Y Yb Lu

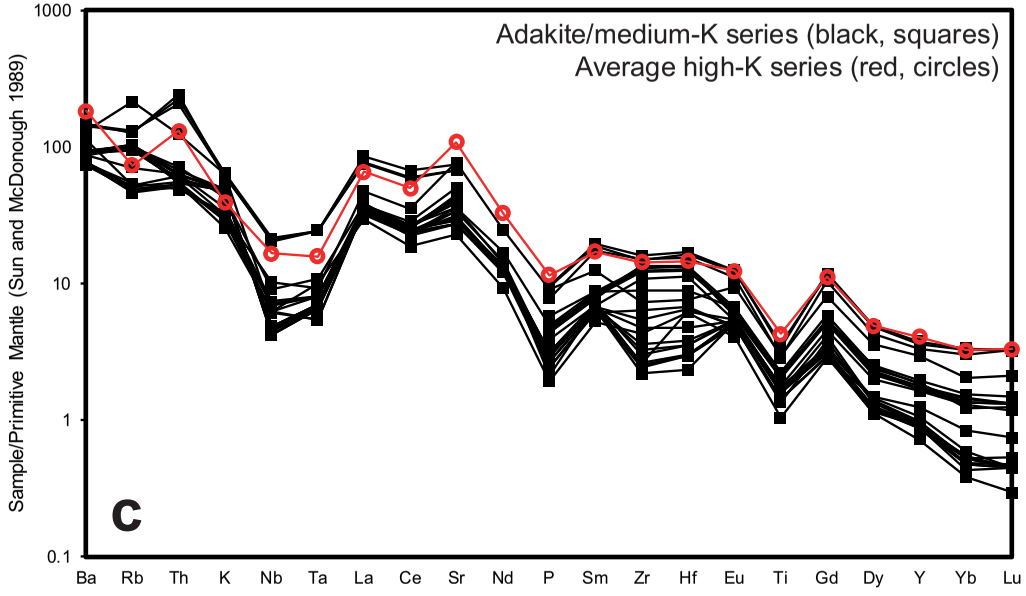
Adakite/medium-K series (black, squares)
Average high-K series (red, circles)
Sample/Primitive Mantle (Sun and McDonough 1989)
1000
100
10
1
0.1
c
Ba Rb Th K Nb Ta La Ce Sr Nd P Sm Zr Hf Eu Ti Gd Dy Y Yb Lu

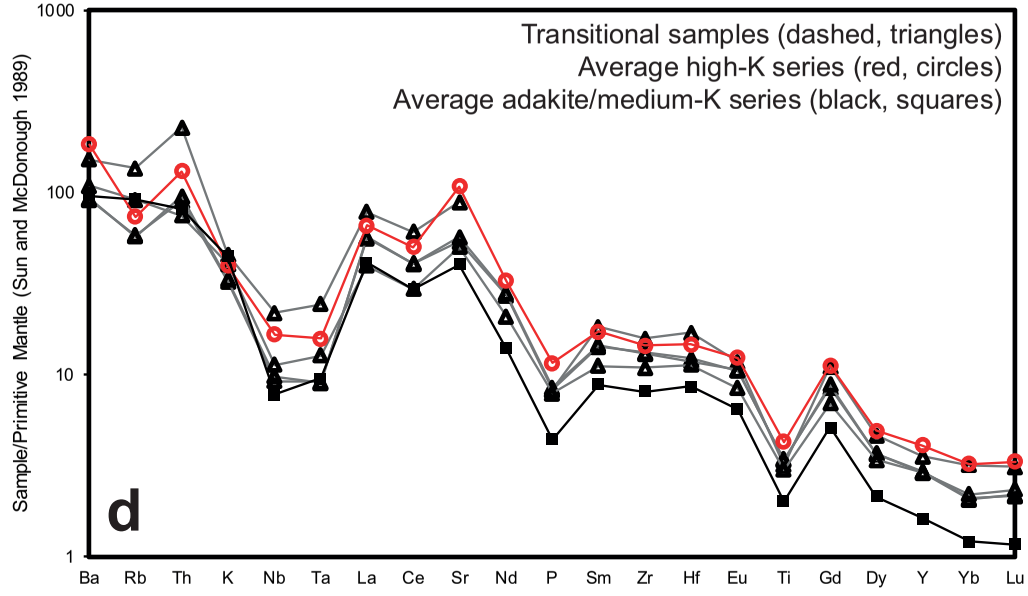
Transitional samples (dashed, triangles)
Average high-K series (red, circles)
Average adakite/medium-K series (black, squares)
Sample/Primitive Mantle (Sun and McDonough 1989)
1000
100
10
1
d
Ba Rb Th K Nb Ta La Ce Sr Nd P Sm Zr Hf Eu Ti Gd Dy Y Yb Lu

Figure 8

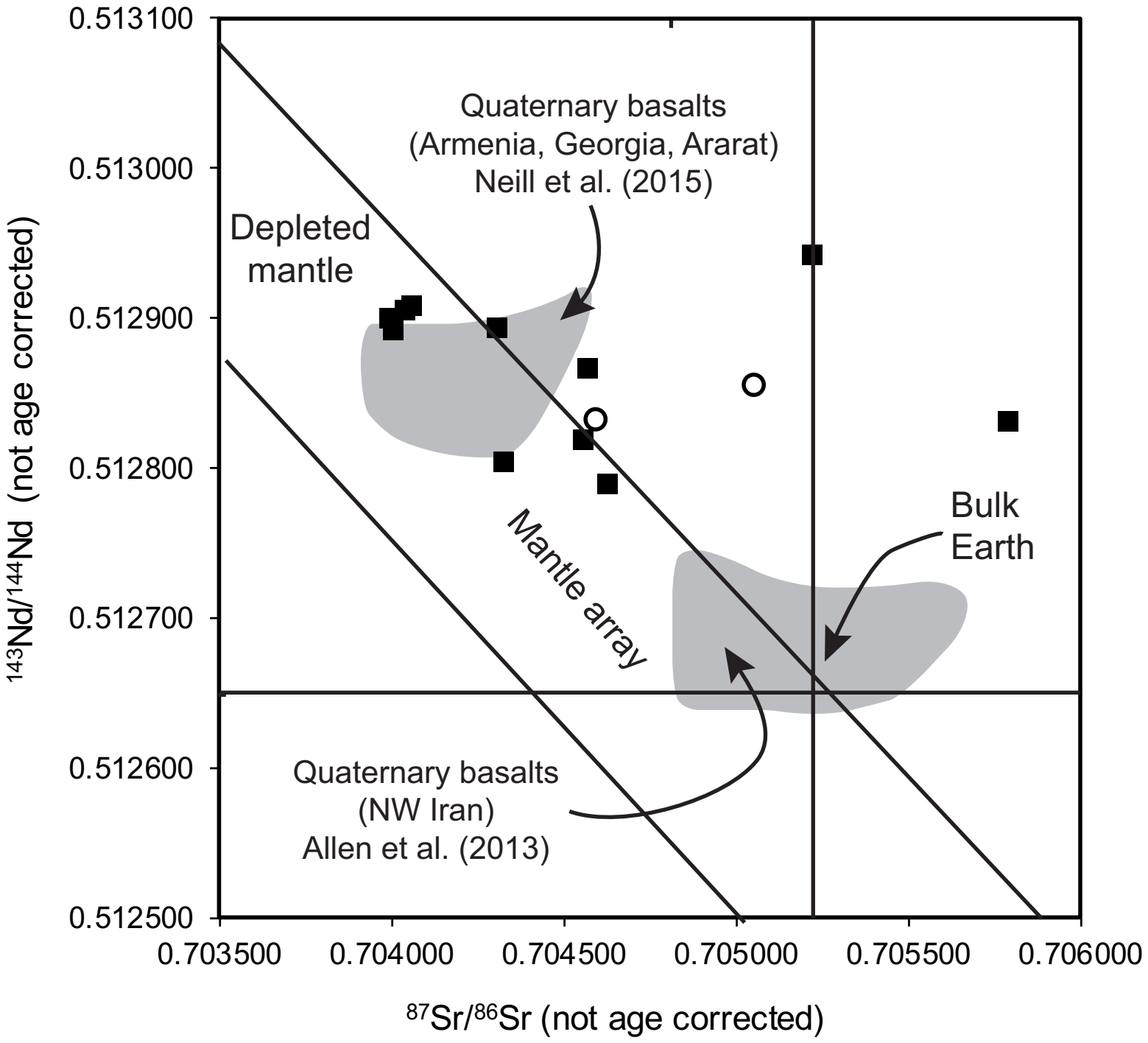
0.513100
0.513000
0.512900
0.512800
0.512700
0.512600
0.512500
143Nd/144Nd (not age corrected)
0.703500
0.704000
0.704500
0.705000
0.705500
0.706000
87Sr/86Sr (not age corrected)
Quaternary basalts
(Armenia, Georgia, Ararat)
Neill et al. (2015)
Depleted
mantle
Mantle array
Bulk
Earth
Quaternary basalts
(NW Iran)
Allen et al. (2013)

Figure 9

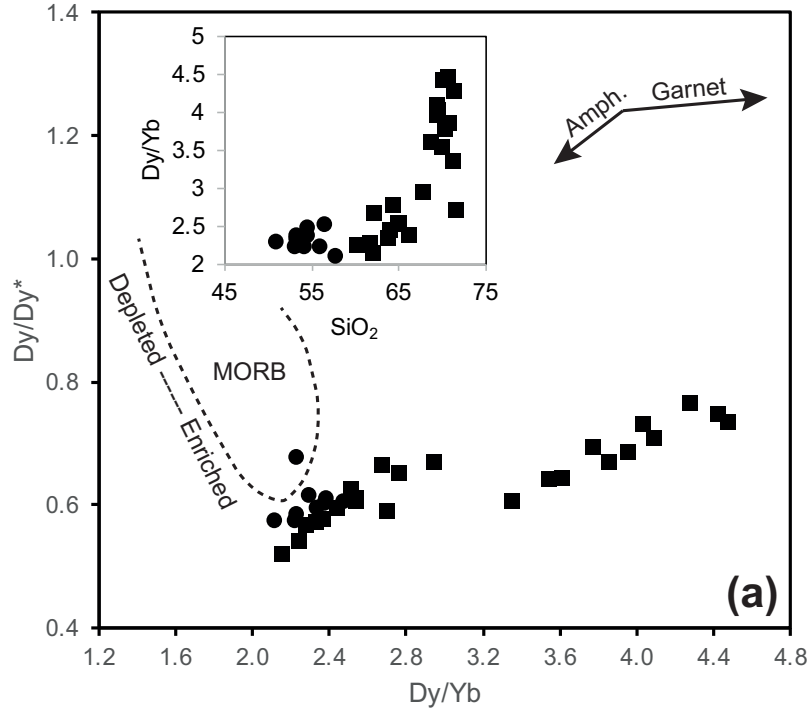
(a)
Dy/Dy*
Dy/Yb
Amph.
Garnet
Depleted
Enriched
MORB
Dy/Yb
SiO2

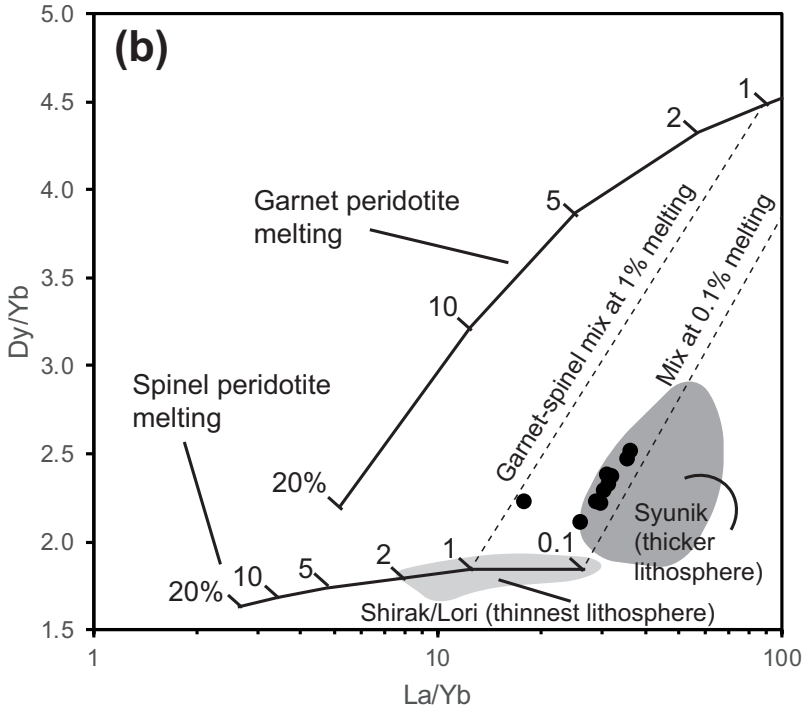
(b)
Dy/Yb
La/Yb
Garnet peridotite melting
Spinel peridotite melting
Garnet-spinel mix at 1% melting
Mix at 0.1% melting
Syunik (thicker lithosphere)
Shirak/Lori (thinnest lithosphere)
20%
10
5
2
1
0.1

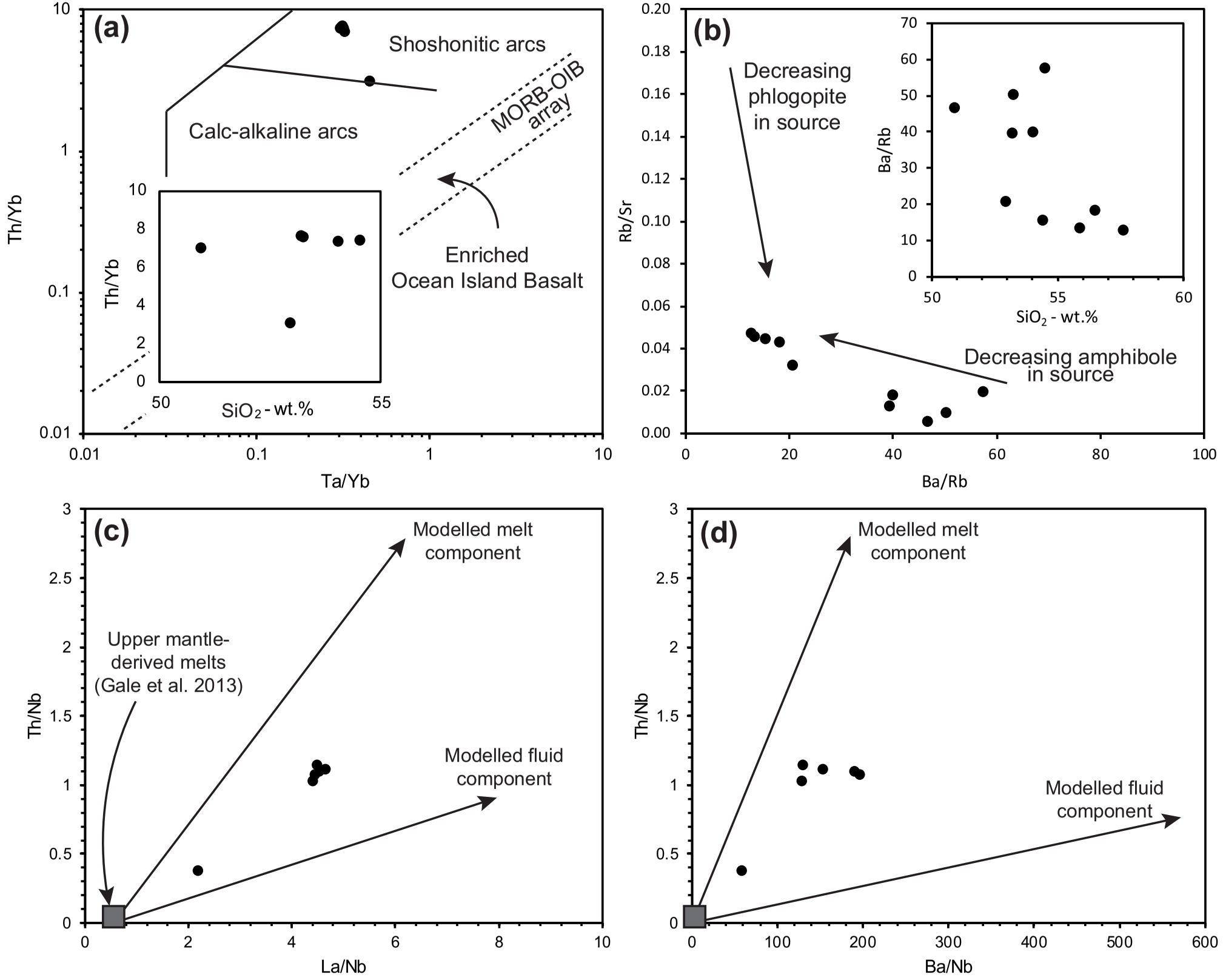
(a)
Shoshonitic arcs
Calc-alkaline arcs
MORB-OIB array
Enriched Ocean Island Basalt
Th/Yb
Ta/Yb
SiO2 - wt.%
(b)
Decreasing phlogopite in source
Decreasing amphibole in source
Rb/Sr
Ba/Rb
(c)
Modelled melt component
Modelled fluid component
Upper mantle-derived melts (Gale et al. 2013)
Th/Nb
La/Nb
(d)
Modelled melt component
Modelled fluid component
Th/Nb
Ba/Nb

Figure 10

Figure 11

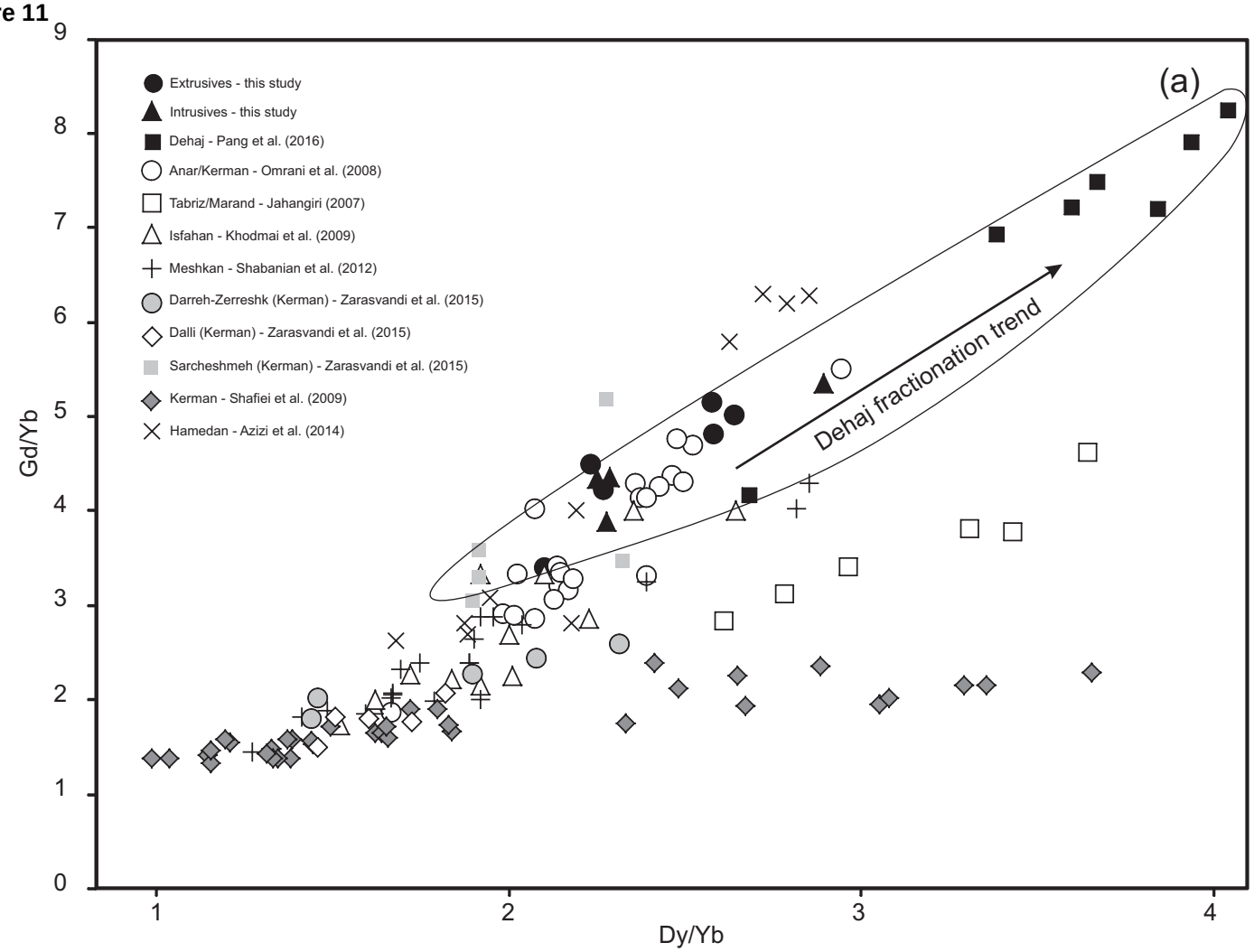

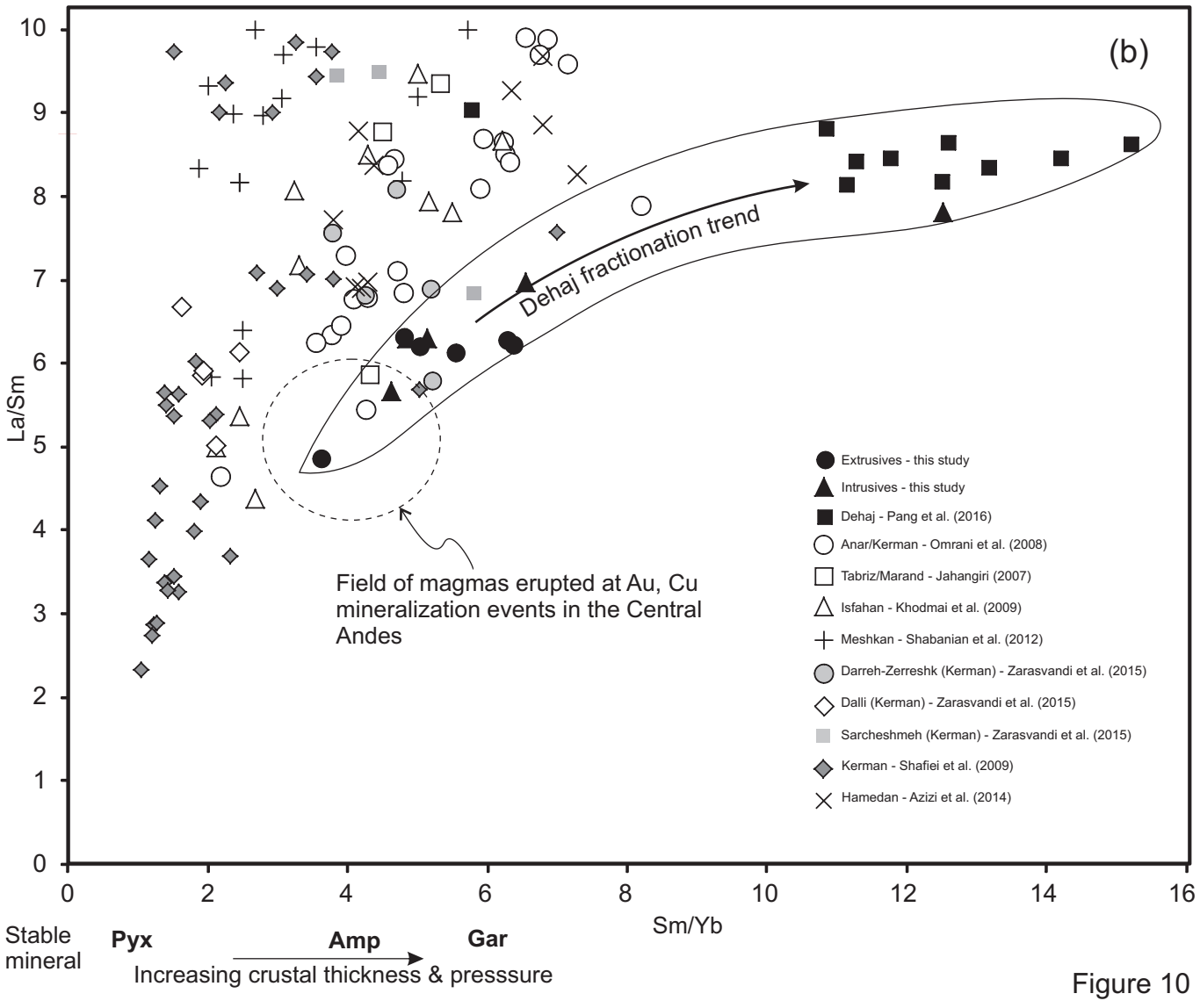

Figure 10

Table 1

Table 1. Kheirkhah et al. Caption in main text.

Sample	**DJ1.1**	**DJ2.1**	**DJ2.2**	**DJ6.1**	**DJ6.2**	**DJ25.1**	**DJ25.5**	**DJ25.7**	**DJ3.3**	**DJ4.1**	**DJ5.1**	**DJ5.4**	**DJ7.1**
Type	**Flow**	**Flow**	**Flow**	**Flow**	**Flow**	**Flow**	**Flow**	**Flow**	**Dome**	**Dome**	**Dome**	**Dome**	**Dome**
Lat.	30.721	30.7	30.7	30.752	30.752	30.753	30.753	30.753	30.687	30.67	30.746	30.746	30.84
Long.	54.76	54.755	54.755	54.707	54.707	54.708	54.708	54.708	54.784	54.889	54.791	54.791	54.867
Series	HK	Transit'	Transit'	HK	HK	HK	HK	HK	Transit'	Adakite	Adakite	Adakite	Adakite
Major oxides (wt. %)													
SiO_2	52.96	60.79	59.95	50.93	54.52	53.20	53.25	54.03	61.77	67.71	71.38	62.16	69.45
TiO_2	0.97	0.69	0.68	0.82	0.83	0.88	0.82	0.78	0.60	0.43	0.27	0.60	0.32
Al_2O_3	16.23	17.06	16.67	15.28	15.91	15.39	15.48	15.84	16.84	16.54	15.30	17.04	15.59
Fe_2O_3	7.47	5.20	5.23	6.63	6.61	6.53	6.36	6.45	4.69	2.26	1.71	4.63	1.98
MnO	0.13	0.08	0.08	0.13	0.12	0.12	0.12	0.12	0.07	0.02	0.03	0.08	0.04
MgO	6.26	3.14	3.43	4.51	5.87	4.61	4.70	4.75	2.42	0.31	0.43	1.69	0.69
CaO	9.13	6.06	6.52	10.99	8.00	9.36	9.12	9.06	5.47	4.10	2.87	5.67	3.43
Na_2O	4.25	4.95	4.89	4.28	4.50	4.29	4.41	4.50	4.88	4.95	4.19	5.53	5.01
K_2O	1.62	1.87	1.92	1.89	2.15	2.46	2.27	1.835	2.34	2.46	2.85	1.84	2.77
P_2O_5	0.42	0.34	0.35	0.51	0.51	0.58	0.53	0.47	0.33	0.20	0.09	0.37	0.12
LOI	0.85	0.37	0.56	2.81	0.60	1.91	1.93	1.98	0.62	1.34	1.03	0.50	0.85
Total	100.38	100.56	100.30	99.31	99.71	99.54	99.38	99.96	100.05	100.35	100.41	100.37	100.30
Trace elements (ppm)													
Sr	1029	1071	1129	5095	1718	3104	3673	1681	1001	713.7	721	1532	673.4
Ba	689	600	610	1309	1938	1574	1861	1237	718	599	623	744	608
Y	18.0	12.5	12.7	18.6	18.5	18.9	18.4	18.1	12.5	8.1	4.0	12.6	4.2
Zr	112	139	137	144	157	171	158	147	114	93	57	77	34
Co	31.4	16.7	17.9	30.2	26.8	28.0	29.0	26.1	14.5	4.4	3.0	12.6	4.2
Ni	136.1	54.9	72.3	173.0	148.4	160.6	157.1	135.6	40.1	b.d.	b.d.	5.3	b.d
V	161.0	114.5	116.7	83.7	160.5	109.2	124.2	126.8	96.4	53.9	27.3	88.7	28.3
Cr	323.7	54.8	82.6	260.1	231.1	244.9	233.1	222.0	51.6	7.8	1.8	7.5	3.0
Zn	71.9	68.4	69.2	66.9	76.6	74.1	71.7	69.0	70.8	35.0	37.7	57.3	45.1
Cu	43.5	53.5	76.5	38.2	46.3	73.8	42.1	58.7	33.0	10.5	24.7	3.4	19.7
Sc	15.2	4.4	5.5	12.1	10.3	10.8	10.7	10.4	3.0	b.d.	b.d.	b.d.	b.d.
Rb	33.3	35.0	34.4	28.0	33.8	40.0	37.0	31.0	54.5	59.5	60.6	31.2	62.3
Nb	11.8	6.1	6.4	10.2	9.9	10.3	9.8	9.5	7.4	6.0	2.8	6.8	3.2
La	25.8	36.3	36.9	30.9	45.0	47.8	44.3	42.8	25.6	24.8	21.1	45.1	43.8
Ce	53.6	68.0	68.5	59.3	85.6	93.0	85.4	81.6	49.5	45.2	39.1	86.1	83.8
Pr	6.2	7.4	7.5	6.7	9.3	10.3	9.4	9.0	5.5	4.8	4.1	9.6	9.2
Nd	29.0	34.1	34.7	30.8	42.8	47.9	42.9	41.1	26.0	21.2	17.4	44.1	42.0
Sm	5.3	5.8	5.9	5.0	7.1	7.8	7.2	6.8	4.5	3.6	2.7	7.2	7.0
Eu	1.6	1.6	1.6	1.4	2.0	2.2	2.0	1.9	1.3	1.0	0.8	2.0	2.0
Gd	5.00	4.6	4.8	4.4	6.3	6.8	6.4	6.0	3.8	2.9	2.1	6.1	6.2
Tb	0.6	0.5	0.5	0.5	0.7	0.7	0.7	0.7	0.5	0.3	0.2	0.7	0.7
Dy	3.2	2.4	2.4	2.4	3.5	3.6	3.3	3.3	2.3	1.6	0.9	3.3	3.3
Ho	0.6	0.4	0.4	0.4	0.6	0.6	0.6	0.6	0.4	0.3	0.1	0.6	0.6
Er	1.6	1.0	1.0	1.0	1.6	1.6	1.5	1.6	1.1	0.6	0.3	1.5	1.5
Tm	0.2	0.2	0.2	0.2	0.2	0.3	0.2	0.2	0.2	0.1	b.d.	0.2	0.2
Yb	1.5	0.9	0.9	0.9	1.5	1.5	1.4	1.5	1.0	0.5	0.2	1.4	1.4

Lu	0.2	0.2	0.2	0.1	0.2	0.2	0.2	0.2	0.2	0.1	b.d.	0.2	0.2
Hf	2.93	3.5	3.4	3.8	4.1	4.6	4.3	3.9	3.2	2.5	1.8	2.2	1.0
Ta	0.7	0.3	0.3	0.5	0.5	0.5	0.4	0.5	0.5	0.4	0.3	0.3	0.3
Pb	7.4	10.4	11.1	8.4	13.7	12.7	10.9	10.3	13.3	11.7	16.7	11.4	15.4
Th	4.5	7.2	7.6	10.5	10.6	11.5	10.8	10.9	5.9	5.7	5.3	4.8	4.3
U	1.4	1.9	1.9	2.3	2.7	2.6	2.2	2.4	2.2	2.0	1.4	1.5	0.8

Table 2

Table 2. Kheirkhah et al. Caption in main text.

	$^{87}Sr/^{86}Sr$	± 2σ	$^{143}Nd/^{144}Nd$	± 2σ	εNd	SiO_2 – wt.%	Series
DJ1.1	0.704590	4	0.512832	5	+3.78	53	High-K
DJ4.1	0.704565	8	0.512865	7	+4.43	68	Adakitic
DJ5.1	0.705217	8	0.512942	5	+5.93	71	Adakitic
DJ5.4	0.704624	7	0.512788	5	+2.92	62	Adakitic
DJ6.2	0.705052	10	0.512855	5	+4.23	55	High-K

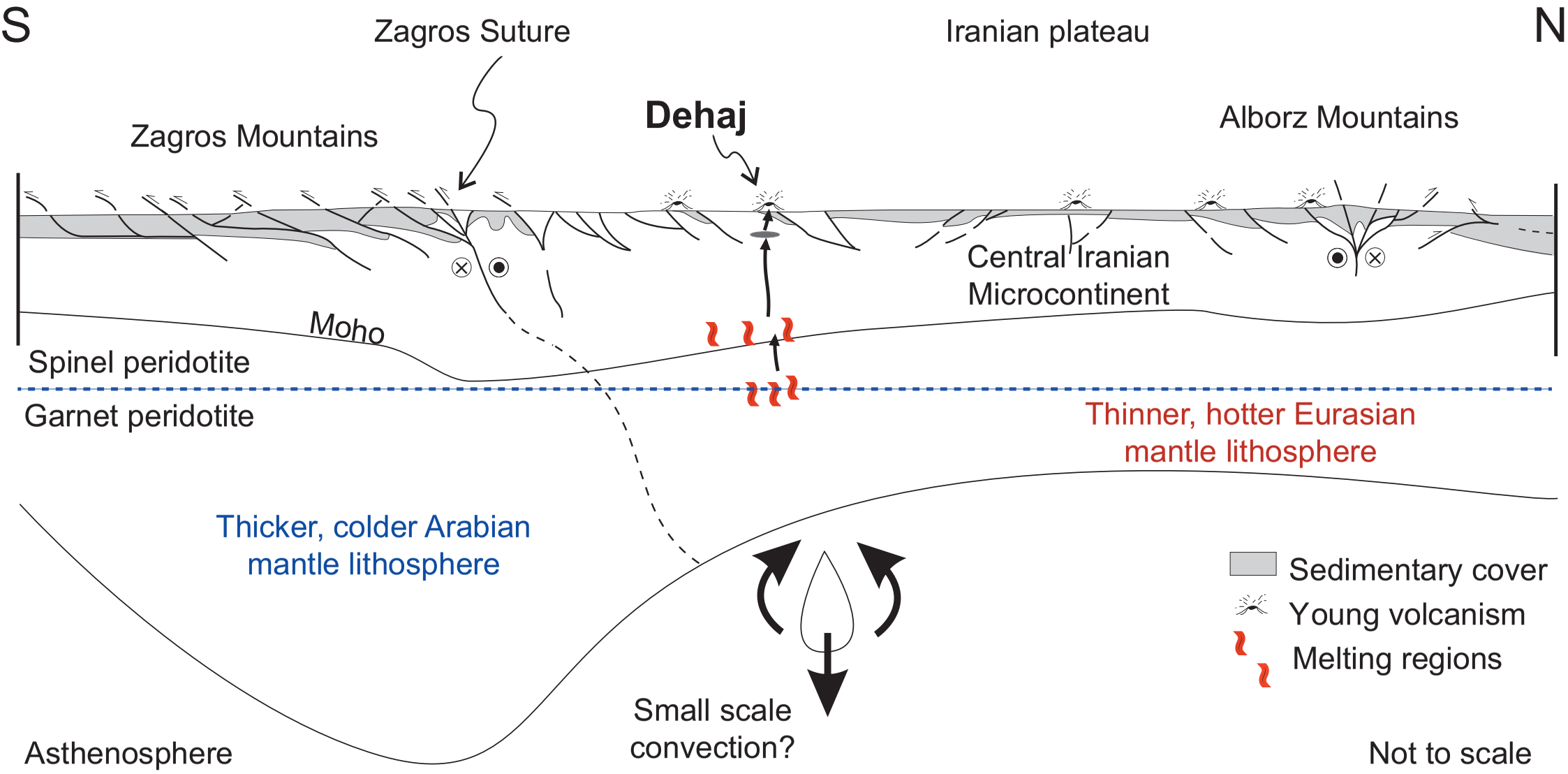
S
N
Zagros Suture
Iranian plateau
Zagros Mountains
Dehaj
Alborz Mountains
Central Iranian
Microcontinent
Moho
Spinel peridotite
Garnet peridotite
Thinner, hotter Eurasian
mantle lithosphere
Thicker, colder Arabian
mantle lithosphere
Sedimentary cover
Young volcanism
Melting regions
Small scale
convection?
Asthenosphere
Not to scale

***Declaration of Interest Statement**

Declaration of interests

☒ The authors declare that they have no known competing financial interests or personal relationships that could have appeared to influence the work reported in this paper.

☐The authors declare the following financial interests/personal relationships which may be considered as potential competing interests:

***Credit Author Statement**

CRediT Author Statement for **JAES-D-19-00942R1**

Monireh Kheirkhah: Conceptualization; data curation; funding acquisition; investigation; project administration; resources; validation; original draft

Iain Neill: Data curation; formal analysis; investigation; methodology; validation; visualization; original draft; review & editing

Mark B. Allen: Conceptualization; Funding acquisition; investigation; project administration; supervision; validation; visualization; original draft; review & editing

Mohammed H Emami: Investigation

Ali Shahraki Ghadimi: Investigation